Geomorphic imprint of high mountain floods: Insight from the 2022 hydrological extreme across the Upper Indus terrain in NW Himalayas

Abhishek kashyap[1], Kristen L. Cook[2], Mukunda Dev Behera[1*]

[1]Centre for Ocean, River, Atmosphere and Land Sciences (CORAL), Indian Institute of Technology Kharagpur, Kharagpur- 721302, West Bengal, India

~~[2]ISTerre~~ [2]IRD, ISTerre, Université Grenoble Alpes, 1381 Rue de la Piscine, 38610 Gières, France

Emails:

Abhishek Kashyap: ~~kashyap95abhishek@kgpian.iitkgp.ac.in~~kashyap95abhishek@kgpian.iitkgp.ac.in

Kristen L. Cook**:** ~~kristen.cook@univ-grenoble-alpes.fr~~kristen.cook@univ-grenoble-alpes.fr

(*Correspondence): Mukunda Dev Behera: ~~mdbehera@coral.iitkgp.ac.in~~mdbehera@coral.iitkgp.ac.in

Style Definition: Header: Font: (Default) Arial,

Style Definition: Footer: Font: (Default) Arial,

Formatted: Space Before: 12 pt, After: 12 pt

Formatted: Font: 16 pt

Formatted: Font: 16 pt

Formatted: Font: 12 pt

Formatted: Font: 16 pt

Formatted: Not Superscript/ Subscript

Formatted: Font: 16 pt

Formatted: Line spacing: Multiple 1.15 li

Geomorphic imprint of high mountain floods: Insight from the 2022 hydrological extreme across the Upper Indus terrain in NW Himalayas

Abstract

- The interaction of tectonics, surface processes, and climate extremes impacts how the landscape responds to extreme hydrological events. An anomalous precipitation event in 2022 occurred during the monsoon season along the lower middle reaches of the Upper Indus River, resulting in short-lived high-magnitude flooding and socioeconomic disruption downstream. To understand the spatial relationship between the geomorphic response and climatic controls of this flood event, as well as their primary triggers, we performed a landscape analysis using topographic metrics and quantified the causal association between hydro-climatic variables. Temperature anomalies in upstream glaciated sub-catchments had a considerable impact on snow cover distribution, based on our observations. As snow cover changed, glacial melt runoff rose, contributing to increased fluvial stream power after traversing higher-order reaches. The higher-order reaches of the Upper Indus River received an anomalously high amount of precipitation, which, when combined with substantial glacial ~~and~~ melt discharge, contributed to an extreme flood across the high-relief steep gradient channels. The flood-affected regions had a high mean basin k_{sn} and SL-index, including

Formatted: Centered, Line spacing: 1.5 lines

Formatted: Space Before: 12 pt, After: 12 pt

Formatted: Subscript

numerous spikes in their magnitudes along their channel profiles downstream. To determine how the lower middle reaches of the Upper Indus River responded to this flood event, we employed the Enhanced Vegetation Index (EVI) and Normalized Difference Water Index (NDWI) as change indicator metrics. We observed an inverse causal influence of NDWI on EVI and a statistically significant relationship between anomalous stream power and relative EVI, suggesting that downstream channel morphology changed rapidly during this episodic event and highlighting EVI as a useful indicator of geomorphic change. We suggest that this extreme flood event is a result of the interaction of anomalous glacial melt and anomalous precipitation over a high-relief landscape, with a certain causal connection with anomalous temperature over the event duration. The synoptic observations suggest that this meteorological condition involves the interaction of the Indian Summer Monsoon (ISM) and Western Disturbance (WD) moisture fluxes. However, the geomorphic consequences of such anomalous monsoon periods, as well as their influence on long-term landscape change, are still unclear.

Keywords: anomalous precipitation; extreme flood; causal relationship; Upper Indus terrain

1. Introduction

High mountain floods in the Himalayas are associated with several processes, including coupling of the Indian Summer Monsoon (ISM) and western disturbance (WD) circulations (Houze et al., 2011), cloudbursts (Dimri et al., 2016), anomalous precipitation, cloud-scale interconnected atmospheric anomalies (Dimri et al., 2017), and geomorphic driven surface processes (Sharma et al., 2017). There is growing recognition that landscapes may evolve through the cumulative effects of extreme episodic events, in particular in rapidly eroding terrains (Korup, 2012; Cook et al., 2018). Recent studies suggest that even minor shifts in weather patterns can have a significant impact on the frequency and magnitude of floods (Knox, 2000; Liu et al., 2015; Benito et al., 2015; Sharma et al., 2022). It has also been suggested that high-magnitude flood occurrences in the bedrock rivers draining the Himalayas are the geomorphic agents with the most significant impact on the evolution of the regional landscape as well as on the residents of the downstream regions (Bookhagen et al., 2005a; Sharma et al., 2017; Panda et al., 2020).

The Tibetan Plateau and its surrounding mountainous regions, such as the Himalayas and the Karakoram ranges, are critical for the downstream hydrology and water availability of the

Formatted: Font: Times New Roman

Indus River system (Hewitt, 2009; Immerzeel et al. 2010) (Fig.1). The majority of the hydrological budget of Indus River comes from precipitation, snowmelt, and glaciers, but their relative contribution varies among the major contributing tributaries (Bookhagen and Burbank 2010; Wu et al., 2021). The Upper Indus catchment- receives precipitation from two distinct climatic systems, the WD and the ISM, over its foreland and highlands in the northwest (NW)- Himalayas (Bookhagen and Burbank 2006; 2010). However, it remains unclear yet how these two distinct circulation patterns interact over the Himalayan landscape and what is their potential influence on long-term geomorphic change (Dimri et al., 2015;2017; Ray et al., 2019).

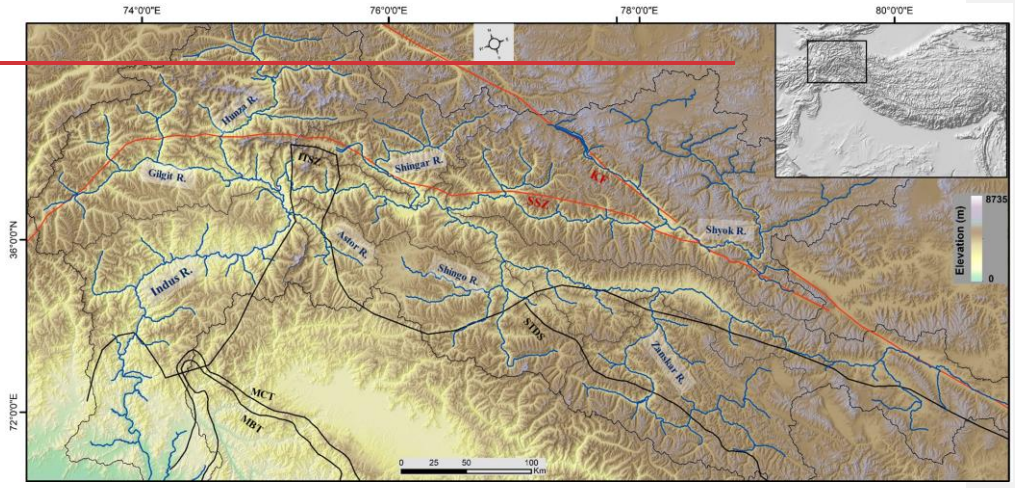

Formatted: Font color: Auto

Formatted: Font color: Auto

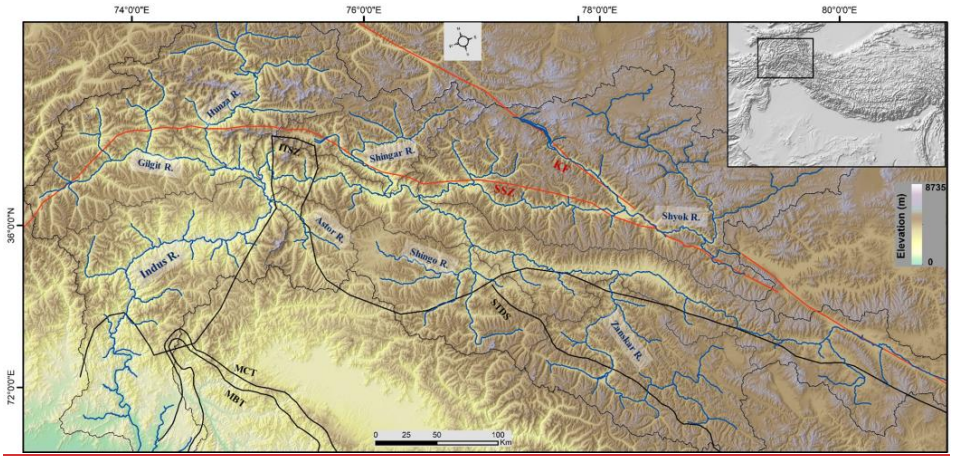

Fig.1. Regional topographic setting of Upper Indus catchment along with its major tributaries overlaid with major geological structures (MBT= Main boundary Thrust, MCT= Main Central Thrust, STDS= Southern Tibet Detachment system, ITSZ= Indus Tibetan Suture Zone, SSZ= Shyok Suture Zone, KF= Karakoram fault~~):~~).

Short-duration episodic weather events have a significant influence on hillslope-surface processes and rates of bedrock erosion by modulating mass movement and subsequent landscape evolution (Snyder et al., 2003; Bookhagen et al., 2005b; Srivastava et al., 2017). During such events, a lot of sediment is transported through the fluvial system, some of which is temporarily deposited in low-gradient reaches and changes the landscape, before being finally deposited in oceanic sinks (Goodbred, 2003; Panda et al., 2020). The geomorphic signatures of catchment morphology are vital for understanding and identifying the channel response involved in such events as well as the processes and patterns of erosion (Kashyap and Behera., 2023; Sharma et al., 2017).

From the beginning of July until the end of August 2022, large portions of the Indus catchment experienced unprecedented monsoon precipitation (Otto et al., 2023; Nanditha et al., 2023). Some recent studies suggest that the primary trigger of this anomalous precipitation event was an intensely low atmospheric circulation pattern, low sea surface temperatures across the eastern Pacific, and the advent of a La-Nina event (Otto et al., 2023; Nanditha et al., 2023). This extreme

Formatted: Font color: Auto

Formatted: Space Before: 12 pt, After: 12 pt

precipitation event resulted in a catastrophic flood in the low elevation flood plains of the Indus catchment (Jones, 2022; Otto et al., 2023; Ma et al., 2023). This severe flood had an extreme impact over the southern province of Pakistan, causing internal displacement of about ~30–32 million people and the deaths of ~1500–1600 people (Bhutto, 2022; Khokhar, 2022; UNICEF, 2022; Ma et al., 2023). In excess of ~$25–30 billion in economic losses are anticipated (Bhutto, 2022; Otto et al., 2023). According to reports, the flood in 2022 exceeded the peak flow rate of the disastrous 2010 floods that occurred over Pakistan (Bhutto, 2022; UNICEF, 2022; Nanditha et al., 2023). The magnitude of the fluvial discharge over the upstream tributaries of the Indus River increased predominantly as a result of increased streamflow across glaciated channels (NDMA, 2022; UNICEF, 2022). However, the geomorphic consequences and the main drivers of this high-magnitude flooding in the Upper Indus catchment have not been evaluated yet.

In the present study, we evaluated the spatial distribution of channel changes in the mountainous portion of the Upper Indus catchment due to the extreme precipitation event in the months of July and August 2022. We employed a channel slope-discharge product along the trunk channel of the Upper Indus River to estimate the anomalies in the stream power resulting from the anomalous precipitation event during July and August 2022. We used a random-forest-based machine learning approach to compare the observed and predicted intensity of precipitation and runoff by assessing the mean climatology of independent hydro-climatic variables. We further quantified the causal relationship between hydro-climatic drivers using nonlinear time series data over the event duration. We investigated the channel response of this episodic flood event by using the NDWI and EVI as change indicator metrics and comparing that to event characteristics such as anomalous precipitation, stream power, and channel metrics. We want to better understand the controls on where and when these types of extreme hydrological events will substantially modify rivers and landscapes so associated geomorphic hazards can be better anticipated, and we also want to better constrain the potential role of these episodic events in driving long-term geomorphic change across the western syntaxial region.

2. Regional Setting

In the Himalayas, the erosion rates are high and the landscape of the mountainous terrain is shaped by the interactions between river systems and the basement tectonics (Jaiswara et al., 2019; 2020).

Among the Himalayan River systems, the Upper Indus is unique, including a fully developed, ~1200-1400 km long, 8th- 9th-order drainage that enters the Himalayan terrain as an antecedent channel and cuts right over the seismically active belt in the Indus- gorges (Fig. 1). This catchment is highly affected by recurrent landslides or debris flows, and episodic glacial and landslide dams that represent significant geomorphic hazards (Korup & Montgomery 2008; Korup et al., 2010).

The Upper Indus River flows through the highly tectonically active region of the Nanga Parbat-Haramosh Massif (NP-HM), which is one of the highest relief regions on earth (~>5000 m), and has the strong potential to rapidly erode uplifted material (Leland et al. 1998; Shehzad et al. 2009; Korup et al. 2010). The NP-HM region experiences the highest recorded rates of denudation and channel incision on earth (~12 mm/y), as well as high rates of tectonic uplift (~4 - 10 mm/y) and forms river anticlines across extremely weak crust (Koons et al., 2002; 2013; Zeitler et al., 2001; 2014; Butler, 2019). This has a significant impact on the tectonics and morphology of the western Himalayas (Hewitt, 2009; Zeitler et al., 2014). The Upper Indus catchment (UIC) is characterized by extremely steep channel gradient of ~>20-25º, high topographic relief of ~4000–5000 m, and a large portion of snow-covered peaks (Hewitt, 2007; Farinotti et al., 2020).

As a fraction of the total annual discharge, snowmelt constitutes up to 50% in the Upper-Indus catchment (UIC) (Burbank & Bookhagen, 2006; 2010; Scherler et al., 2011). Due to the Western Disturbance (WD) inclination, the UIC has a lot of precipitation in the winter and spring (Kapnick et al., 2014), while due to the orographic barrier of the high mountains, the influence of the ISM in the region weakens towards to the north-west (Forsythe et al., 2017). The annual precipitation in the UIC increases with the elevation; across the northern valley floors- in the rain shadows it ranges from 100-200 mm/y; while at elevation ~4000-4400 ma.s.l., it ranges from 600-800 mm/y; and above >~5000 ma.s.l., it ranges from 1500 -2000 mm/y (Sharif et al., 2013; Wu et al., 2021). From October to March, the monthly mean temperatures in the UIC are below freezing at elevations > ~3000 m (Archer, 2004). Discharge in the tributary channels of the Upper Indus River that depend on glacier meltwater has a strong association with summer time mean air temperatures across the Karakoram ranges (Forsythe et al., 2017; Wu et al., 2021).

3. Materials and Methodology

3.1 Data Used

Formatted: Font: Times New Roman, 12 pt

Formatted: Font: Times New Roman

In the present study, we used a 30 m SRTM digital elevation model (DEM) for landscape characterization and geomorphic quantative parameter estimation. ~~In order to~~To investigate ~~how~~the impact of the climatic variables driving this extreme event ~~affect the processes of~~on regional erosion processes, we ~~used 40 years' (1982–2022) duration of~~utilized daily precipitation datasets spanning 40 years (1982–2022) from ~~the~~ July 1 to August 31 ~~period~~ from CHIRPS (Climate Hazards Group Infrared Precipitation with Station Data) (Version 2.0 Final). ~~Using the climatology of daily~~Several previous studies have investigated CHIRPS precipitation datasets at daily, monthly, and annual temporal scales across the Indus Basin (Gao et al., 2018; Ullah et al., 2019; Nawaz et al., 2021; Shahid et al., 2021). In their studies, they extensively evaluated CHIRPS's performance against regional ground datasets obtained from ~~July 1 to August 31, we observed the~~meteorological stations. Several studies (Katsanos et al., 2016, Paredes-Trejo et al., 2017, Bai et al., 2018, Gao et al., 2018) suggest CHIRPS for hydrological analysis and water resource management due to its fine spatiotemporal ~~occurrence of hydro-meteorological variables. These variables included 2-m air temperature, skin temperature, dewpoint temperature, snowmelt, and runoff acquired from ERA5-Land Daily Aggregated-ECMWF Climate Reanalysis with a spatial~~ resolution ~~of 11132 meters. We used remote sensing based indices, such as MODIS-derived normalized difference water index (NDWI), normalized difference snow index (NDSI), snow albedo, EVI, and surface reflectance bands b1 and b2, with a spatial resolution of 500 meters, for anomalous change indicators.~~ .

We investigated the spatiotemporal distribution of hydrometeorological variables using daily datasets from July 1 to August 31. The ERA5-Land Daily Aggregated-ECMWF Climate Reanalysis, which had a spatial resolution of 11132 meters, provided data on 2-meter air temperature, skin temperature, dewpoint temperature, snowmelt, and runoff. We used remote sensing-based indices to detect signatures of anomalous changes over the landscape. We computed these metrics over the monthly mean for July and August 2022, using daily datasets of the MODIS-based normalized difference water index (NDWI), the normalized difference snow index (NDSI), snow albedo, EVI, and surface reflectance bands b1 and b2, which have a 500-meter spatial resolution.

3.2 Drainage network extraction and landscape analysis.

Formatted: Space Before: 12 pt, After: 12 pt

We extracted the drainage network from the DEM using the ArcGIS platform. A regional slope map was produced by running a 1000 m radius mean filter over the slope model derived from the DEM, and a regional relief map was generated by passing a 1000 m circular radius focal range window over the DEM. Further analysis of the DEM and the derived flow accumulation data were performed in MATLAB using the transient profiler tools (Jaiswara et al., 2019, 2020). We extracted the longitudinal profiles of the bedrock channels within an accumulation region of about $1*10^6$ m^2 and channel network of the Upper Indus catchment using TopoToolbox (Wobus et al., 2006; Kirby and Whipple, 2012; Schwanghart and Scherler, 2014). We used a 1000 m smoothing window and a 20 m vertical interval to sample the channel networks in order to reduce the noise and artefacts that are embedded in the elevation data.

3.3 Quantitative Geomorphic parameters

We used geomorphic quantitative parameters such as SL (Stream length-gradient index)-index, k_{sn} (Normalized steepness index) and Stream power of the Upper Indus trunk channel to evaluate the influence of the high magnitude flooding event across the Upper Indus River during July and August 2022. To evaluate the spatial variability of the flood magnitude and the channel morphology, these metrics are plotted on the longitudinal profile of the trunk channel.

3.3.1 Stream length-gradient index (SL- Index)

Rivers often achieve an equilibrium or steady state between erosion and sedimentation, which is represented by a concave longitudinal river profile (Schumm et al., 2002). Tectonic, lithological, and/or climatic factors often result in shifts in river profiles from this expected steady-state condition (Hack, 1973; Burbank and Anderson, 2011). Here, we use the Stream Length-Gradient (SL) index to identify the zones of topographic break and changes in the channel gradient of the longitudinal profile by using the equation:

Formatted: Font: Not Bold

$$\mathbf{SL = (\Delta H/\Delta L)/L \ldots\ldots\ldots\ldots\ldots\ldots (1)}$$

where SL denotes the steepness or gradient of the profile for the local reach, L is the total river length from the midpoint of the local reach to the highest point on the channel, ΔH is the change in elevation over the reach and ΔL is the length of the reach, so $\Delta H/\Delta L$ represent the channel slope

or gradient of the reach. A sharp lithological variation and/or the differential uplift across active structures are frequently linked to an abrupt change in SL-index along the river (Hack, 1973; Jaiswara et al., 2020; Kashyap et al., 2024).

3.3.2 Channel Steepness index

We extracted the bedrock profile of the Upper Indus River, which can be described using the power law relationship between upstream drainage area (A) and channel gradient (S) as (Jaiswara et al., 2019, 2020; Kashyap et al., 2024):

$$S = k_s A^{-\theta} \quad \ldots\ldots\ldots\ldots\ldots\ldots (2)$$

where $k_s = (E/K)1/n$ is the channel steepness index, $\theta = (m/n)$ is the channel concavity index, m and *n* are positive constants, E is the erosion rate at a steady state (Wobus et al., 2006; Kirby and Whipple, 2012). The relative magnitude of k_s is often related to the surface uplift rate as well as the erosional efficiency across a bedrock catchment (Snyder et al., 2003; Wobus et al., 2006).

3.3.3 Stream Power estimation

The normalized steepness index (k_{sn}) has emerged as an important topographic metric with significant correlation with erosion rate over a wide range of timescales (Wobus et al., 2006; Jaiswara et al., 2019; Kashyap et al., 2024). However, one major drawback of k_{sn} is that it includes an assumption of spatially constant precipitation because upstream drainage area is used as a proxy for discharge (Adams et al., 2020; Leonard et al., 2023a).

In the present study, we incorporate the precipitation intensity into the stream power ~~law~~calculation to analyze the anomalous stream power along the trunk channel during the flood event. We estimate the precipitation induced stream power using the slope-discharge method, which involves multiplying the accumulated flow distance weighted by precipitation with the hyperbolic tangent function of the channel gradient along the flow path (Adams et al., 2020; Leonard et al., 2023b). The estimation of stream power ($K_{sn}Q$) as a function of channel discharge can be estimated as:

Formatted: Font: Times New Roman
Formatted: Font: Times New Roman
Formatted: Font: Times New Roman
Formatted: Font: Bold, Font color: Auto
Formatted: Space Before: 12 pt, After: 12 pt
Formatted: Font color: Auto

$$K_{sn}Q = (S) \times f(\int p * FD) \ldots\ldots (3)$$

where S is the channel gradient, FD is the accumulated flow distance, p is the accumulated precipitation (Leonard et al., 2023a; b). Thus, $K_{sn}Q$ is a normalized version of the channel steepness metric that uses the product of channel gradient (S) and upstream discharge (Q) estimated from mean precipitation (P) as a fluvial discharge proxy. This enables $K_{sn}Q$ to account for the spatial and temporal variability in precipitation along the upper Indus River during the high magnitude flood event. Accumulated precipitation resolves spatial patterns well and scales nearly linearly with relevant discharges, particularly for large and long-lasting precipitation events (Rossi et al., 2016; Leonard et al., 2023a; b).

3.4 Machine learning based approach to model the anomalous event characteristics

The Random Forest (RF) technique is a supervised machine learning method that has been used as a tree-based ensemble technique and includes a bagging or boot-strapping algorithm (Breiman, 2001; Wolfensberger et al., 2021). In the present study we use a RF based multivariate regression approach to estimate the anomalous precipitation and runoff intensity in July and August 2022 using the independent variables obtained from classifying variable importance.

$$H(x) = \sum_{i=1}^{T} hi(x) \ldots\ldots\ldots\ldots\ldots (4)$$

Where, hi (x) denotes the i^{th} regression tree output (hi) on sample x. Therefore, the prediction of the RF is the mean of the predicted values of all the decision trees. T denotes the regression trees for regression prediction.

Based on the mean climatology of the last 40 years, we predict the daily anomalous precipitation and runoff intensity for the 2022 event and compare them with the observed actual values. We employed the highest significance variables, as well as precipitation and runoff data from 1982 to 2021, as a training set. We utilized a time series cross-validation approach in this study to evaluate the Random Forest model's performance in predicting precipitation and runoff during the Upper Indus catchment's high-elevation flood event in July and August 2022. Given the temporal dependency and sequential pattern of hydro-climatic data, using a normal K-fold cross-validation method could result in data leakage by allowing future data to inform past projections.

Formatted: Font color: Auto
Formatted: Font color: Auto
Formatted: Font color: Auto
Formatted: Font color: Auto
Formatted: Font color: Auto
Formatted: Font color: Auto
Formatted: Font: Not Bold
Formatted: Font color: Auto
Formatted: Font color: Auto

To address this issue, we employed time series cross-validation to maintain the data within chronological order. We trained the model using a sliding window method, gradually moving the training window forward in time with each iteration. Specifically, we designed the first training window to contain data from the first 30 years, leaving the last 10 years for testing. In each successive iteration, we increased the training window by one year and retrained the model on the expanded training set. We trained these models on meteorological variables obtained from the classification of the most significant, as well as other physical drivers associated with high-elevation flood episodes in the region. We evaluated the model's performance based on the accuracy of precipitation and runoff predictions, using metrics such as mean absolute error (MAE), mean squared error (MSE), and root mean squared error (RMSE) (SI. Table. 1- 2). We computed these metrics for each rolling window to gain insight into the model's performance across various time periods, especially in the lead-up to the 2022 flood event. To utilize the independent variables to estimate these event characteristics, we first classify the hydro-climatic variables based on their higher importance using the RF classification approach. Then, by using the RF multivariate regression approach, we select only those independent variables with the highest significance to estimate anomalous precipitation and runoff intensity during the event duration.

Formatted: Font color: Auto

Formatted: Font color: Auto

3.5 Causal discovery among Hydro-climatic variables

Causal methodologies have been utilized to evaluate whether and how changes in one hydro-climatological variable during anomalous extreme events influence the magnitude of another (Runge et al., 2019a; Nowak et al., 2020). To understand how an extreme event is regulated over high mountainous terrain, a temporal investigation of event characteristics is required. Using this evaluation, we gain insight into how the conditioning hydro-climatic variables that regulate these extreme events evolve throughout event duration in a catchment (Runge, 2018; Krich et al., 2020). Understanding directional dependencies is crucial to distinguish them from connections that cannot be deduced using any statistical model (Kretschmer et al., 2017; Karmouche et al., 2023).

In this study, we use causal stationarity, and the absence of contemporaneous causal effects for the time series datasets using the PCMCI and MCI approaches (Tibau et al., 2022; Runge, 2023). PCMCI is a causal identification technique that combines the Momentary Conditional Independence (MCI) approach with the PC algorithm (Runge et al., 2019b; Nowack et al., 2020).

Formatted: Font color: Auto

Given a set of multivariate time series, PCMCI estimates the time series graph that depicts the conditional independencies among the time-lagged factors (Runge et al., 2014; 2019a). In addition to PCMCI, we use the ParCorr linear independence test based on partial correlations is employed (Runge et al., 2014; 2023).

In order to evaluate the meteorological disturbances associated with the Upper Indus Flood of 2022, we identified the causal lag-connection between hydroclimatic variables, with a specific focus on exploring the meteorological conditions leading up to and during the flood event. We focused on identifying the short-term meteorological drivers that triggered the anomalous precipitation-driven high elevation flood and understanding the distribution of its immediate impacts within the Upper Indus catchment. We emphasize that this study does not attempt to explore the causality of long-term climatic changes or assess the full geomorphic consequences of the flood on the landscape. We deliberately limit the scope to comprehend the meteorological conditions and their direct impact on the flood in the July-August 2022 period. By narrowing our focus to the short-term hydro-climatic interactions, we aim to offer insights into the key atmospheric processes and their role in shaping the event's severity rather than its broader or longer-term geomorphic impacts.

In the present study we use the daily datasets of hydro-climatological variables and group them as; Temperature gradient (Tg), including Air temperature, Surface temperature, and Dewpoint temperature; Rainfall gradients (Rg), including Precipitation intensity, Runoff and Snowmelt; and anomalous change indicators (Ac) including EVI, NDWI, and NDSI, July 1 to August 31, 2022, so includes 62 observational intervals. We evaluate the causal interference between these hydro-climatic variables using the MCI approach with a maximum 2-day lag period ($\tau_{max} = 2$) and a limit for significance set to 0.05 ($\alpha = 0.05$), in order to examine the spatially interdependence relationships among each of these variables during 2-day event periods.

3.6 Moisture pathways

The Hybrid Single-Particle Lagrangian Integrated Trajectories (HYSPLIT) model (~~https://www.ready.noaa.gov/HYSPLIT_traj.php~~https://www.ready.noaa.gov/HYSPLIT_traj.php) has been employed to determine the probable moisture parcel source region (Joshi et al., 2023). Over the past decade, researchers have used the HYSPLIT model to identify moisture sources

Formatted: Font: Times New Roman
Formatted: Font color: Auto
Formatted: Font color: Auto
Formatted: Font color: Auto
Formatted: Space Before: 12 pt, After: 12 pt
Formatted: Font: 12 pt
Formatted: Font: 20 pt
Formatted: Font color: Auto
Formatted: Font color: Auto

(Wang et al., 2017; Joshi et al., 2023). To determine the backward trajectory following an anomalous precipitation event, this study used the HYSPLIT model. We used three starting heights of 500, 1000, and 3000 ma.s.l. to calculate the backward trajectory for each day of July and August 2022, given that the HYSPLIT model required the start date/time, location, and height for each precipitation event (Wang et al., 2017; Gudipati et al., 2022). This study used meteorological data with a spatial resolution of 1º×1º from the Global Data Assimilation System (NCEP-GDAS).

4. Results

4.1 Geomorphic analysis of the Upper Indus terrain

The Indus River is around ~1400–1600 km long and forms multiple loops both parallel to and in opposition to the regional structural trend; its bed elevation ranges from ~500-6000–m. The river exhibits distinct morphological characteristics over its flow path in terms of its topographic attributes and derivatives. Over the elevated low-relief landscape in the Tibetan plateau, the relief and channel gradient vary as (~0-500 m; ~0-10°), with a low SL index (~ <1 *10^4) gradient meter and mean basin k_{sn} of (~<90 $m^{0.9}$) (Fig. 2; Fig. 3a). Then, when the river traverses through the NP-HM region, there is a progressive rise in the local relief and channel gradient to (~>2000-3000 m; ~>25-35°), which is also reflected in the SL-index (>2.5-3×10^4) and mean k_{sn} (~>331 $m^{0.9}$). This region is characterized by topographic discontinuities across active structures, leading to high relief variation and topographic roughness.

Formatted: Font color: Auto

Formatted: Font color: Auto

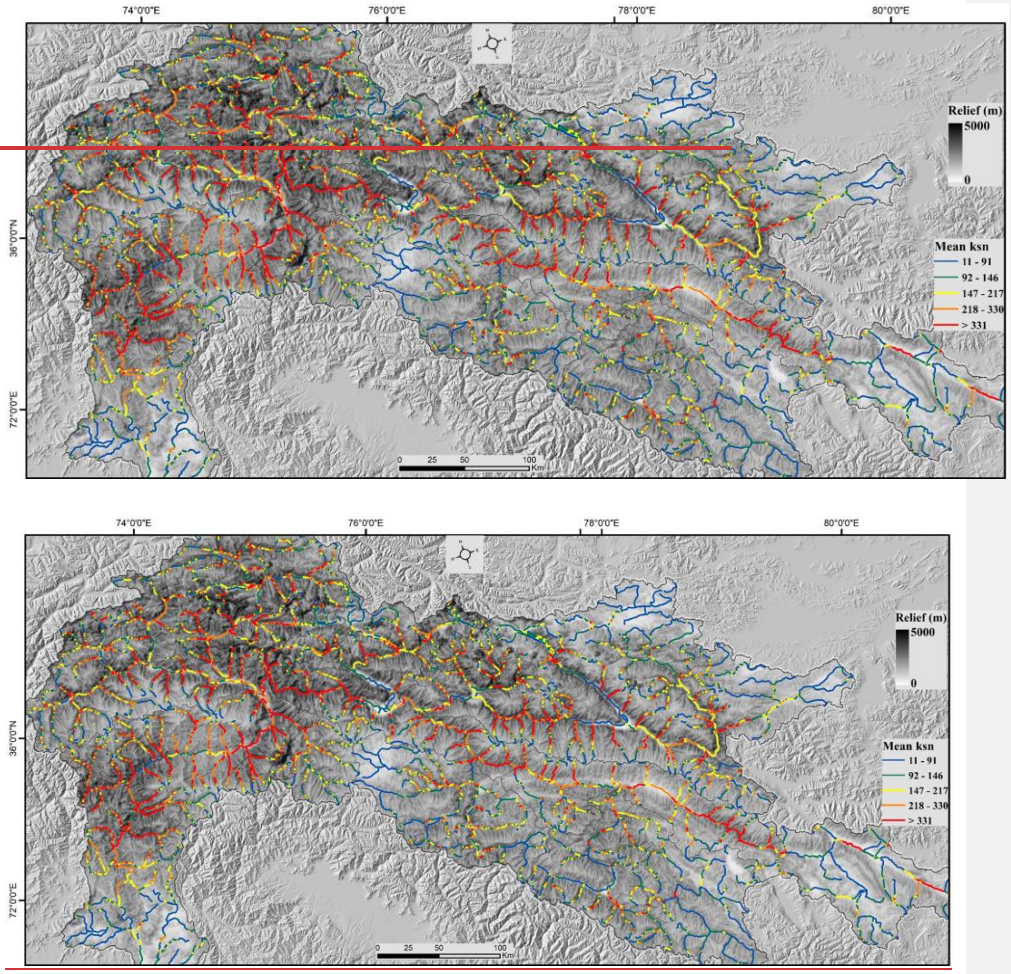

338

339

340 Fig.2. Spatial distribution of local relief overlaid with Mean basin k_{sn} ranges across the Upper
341 Indus River catchment.

342 The tributaries in the upstream glaciated valleys that flow parallel to the structural trend
343 have a higher mean channel gradient (>~20-30º) and topographic relief (>~2000-3000 m) (Fig. 2).
344 When these tributary channels start to descend towards the main stream after following the
345 glaciated landscape, the value of SL and k_{sn} for the trunk channels shows a significant rise at

Formatted: Subscript

Formatted: Font color: Auto

Formatted: Font color: Auto

Formatted: Space Before: 12 pt, After: 12 pt

~3000–4000 m mean elevation. Approaching the southern mountain front, the main trunk channel relief and channel gradient are ~1000-2000 m and ~15-25° respectively (Fig. 3a).

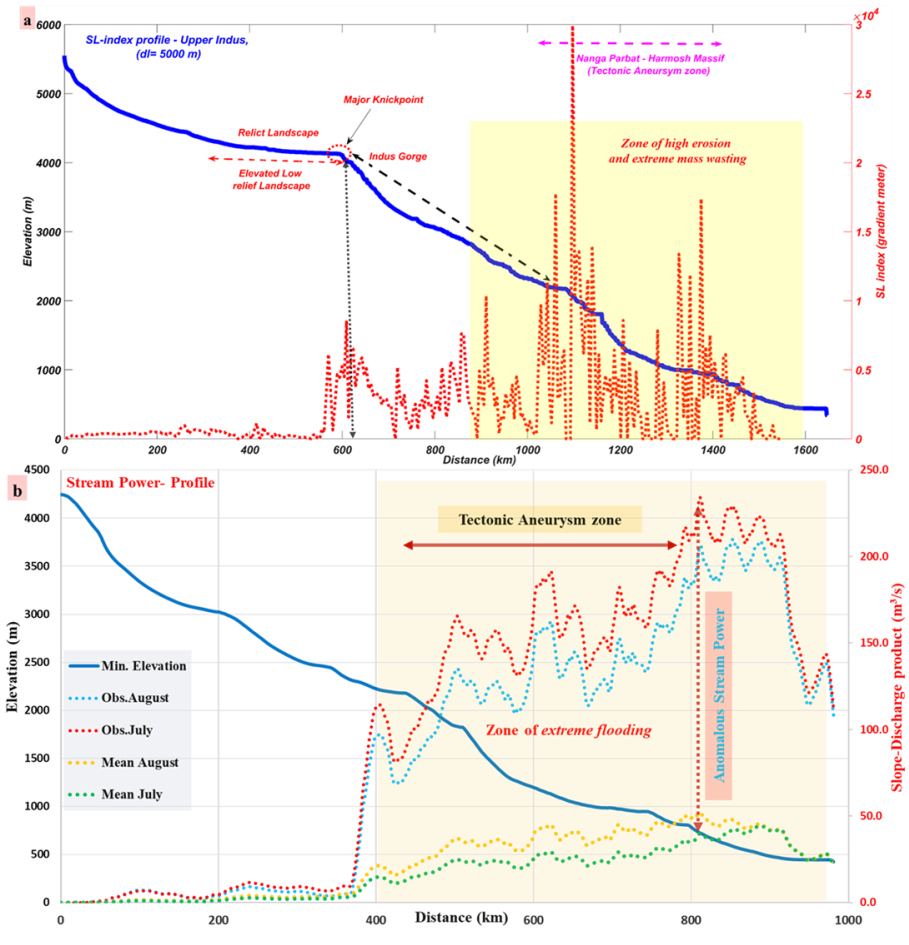

Fig.3. The trunk channel profile of Upper Indus ~~river~~River plotted with (a) SL-index; (b) The highest order profile of Upper Indus ~~river~~River plotted with Stream power (slope-discharge product)-channel elevation (highest order profile is the subset of trunk channel profile indicated by black dash line).

Formatted: Font color: Auto

Formatted: Font color: Auto

The spatial association of higher k_{sn} (>~331 $m^{0.9}$), topographic relief (~1500-2000 m), and longitudinal increase in channel gradient along the main Upper Indus River channel downstream suggests a higher erosional regime. These high values for the various topographic metrics highlight zones of accelerated erosion where the river is in gradational disequilibrium. Furthermore, this tectonically active southern front coincides with a region that gets significant annual mean precipitation (~1500–2500 mm/y), suggesting a tectonic-climate linkage in the erosional process.

Formatted: Font color: Auto

Formatted: Space Before: 12 pt, After: 12 pt

Formatted: Font color: Auto

4.2 Spatial distribution of Hydro-climatic anomalies over event duration

The downstream reach of the Upper Indus trunk channel received a significant amount of anomalous precipitation (>~60–80 mm/d) during the observation period of July and August 2022 (Fig. 4a, 4b). The spatial variability of anomalous precipitation varies with a range of >~0–40 mm/d along its major glaciated tributaries, such as Hunza, Astor, Gilgit, Shingo, and Zanskar. In July and August 2022, the total extent of anomalous precipitation was around ~900–1000 mm/month, which was approximately ~300–400% more than the long-term (1982–2022) mean climatology. From July to August 2022, there was continuous precipitation in the high gradient downstream region, and due to the antecedent weather conditions, extreme precipitation likely produced suitable conditions for high-magnitude flooding. The potential geomorphic response of such anomalous precipitation is suggested by the resulting anomalous stream power over the downstream channels (Fig. 4c, 4d). The spatial distribution of anomalous stream power shows that the greatest increase occurred at ~400-800 km along the channel profile downstream. For both the months of July and August of 2022, we observed a significant rise in the stream power, to ~>200 m^3/s above the mean values (Fig. 3b).

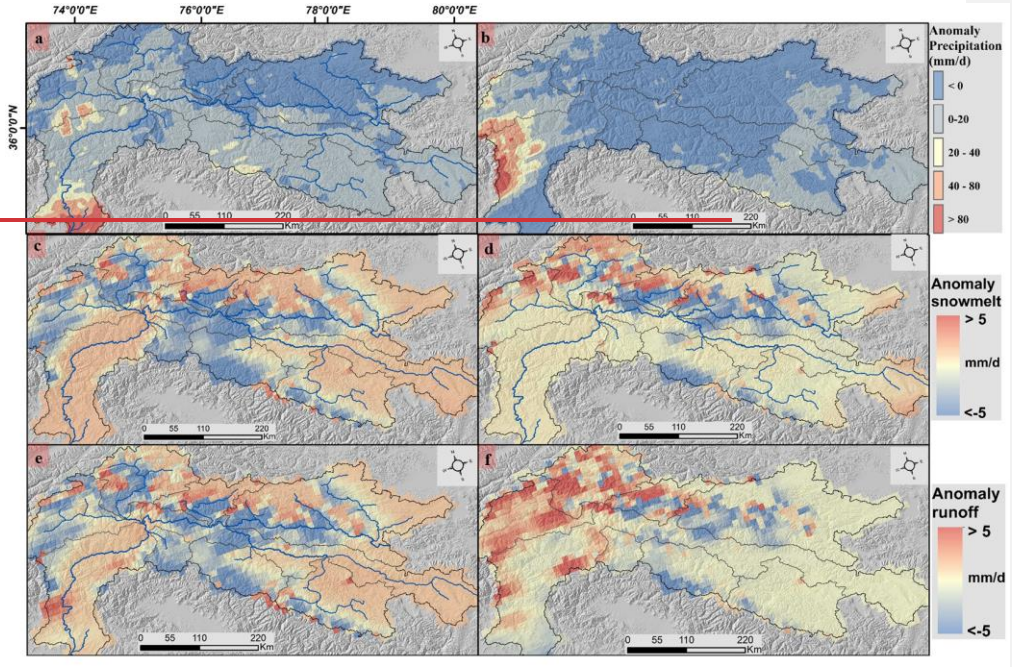
74°0'0"E
76°0'0"E
78°0'0"E
80°0'0"E
36°0'0"N
a
b
c
d
e
f
0 55 110 220 Km
Anomaly Precipitation (mm/d)
< 0
0-20
20 - 40
40 - 80
> 80
Anomaly snowmelt
> 5
mm/d
<-5
Anomaly runoff
> 5
mm/d
<-5

374

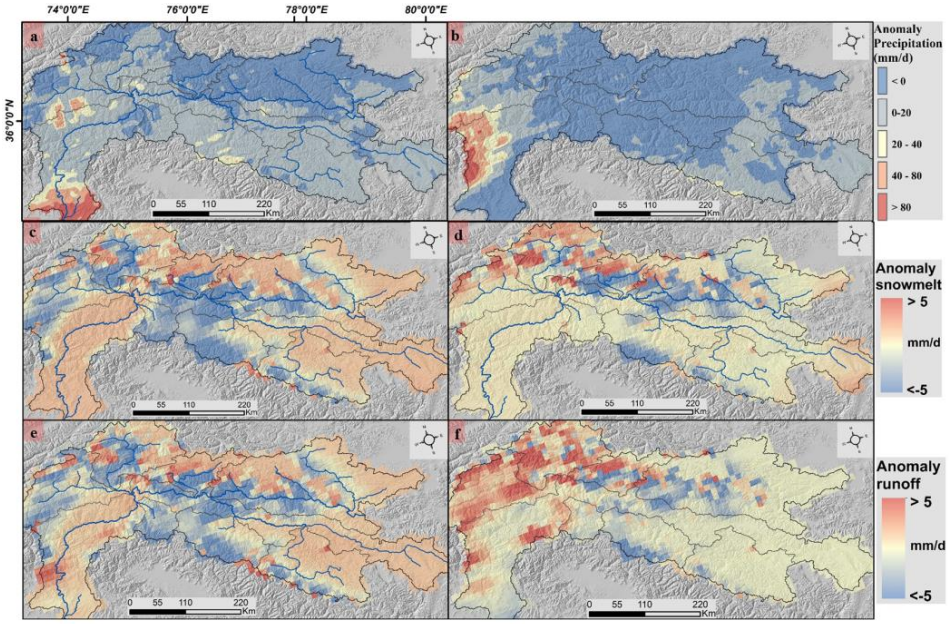

Fig. 4. Spatial distribution of hydro-meteorological variables for anomalous July and August month of 2022 across Upper Indus catchment such as: (a) precipitation (July) (b) precipitation (August) (c) Snowmelt (July) (d) snowmelt (August); (e) Runoff (July) (f) Runoff (August).

During the observation period, other variables, such as runoff and snowmelt, also showed positive anomalies across the upstream glaciated sub-catchments over the Karakoram ranges (Fig. 4e, 4f). Furthermore, during July and August 2022, the temperature variables indicated a positive deviation from the mean climatological trend over the glaciated catchments. In the upstream sub-catchments in Shyok, Shingar, Hunza, and Gilgit, air and dewpoint temperatures reach (>~3°C above mean), while surface temperatures reach (>~6°C above mean) (Fig. 5). The spatial distribution of anomalous temperatures corresponds well with the anomalous snowmelt and runoff magnitude across the upstream glaciated catchments.

Formatted: Space Before: 12 pt, After: 12 pt

387

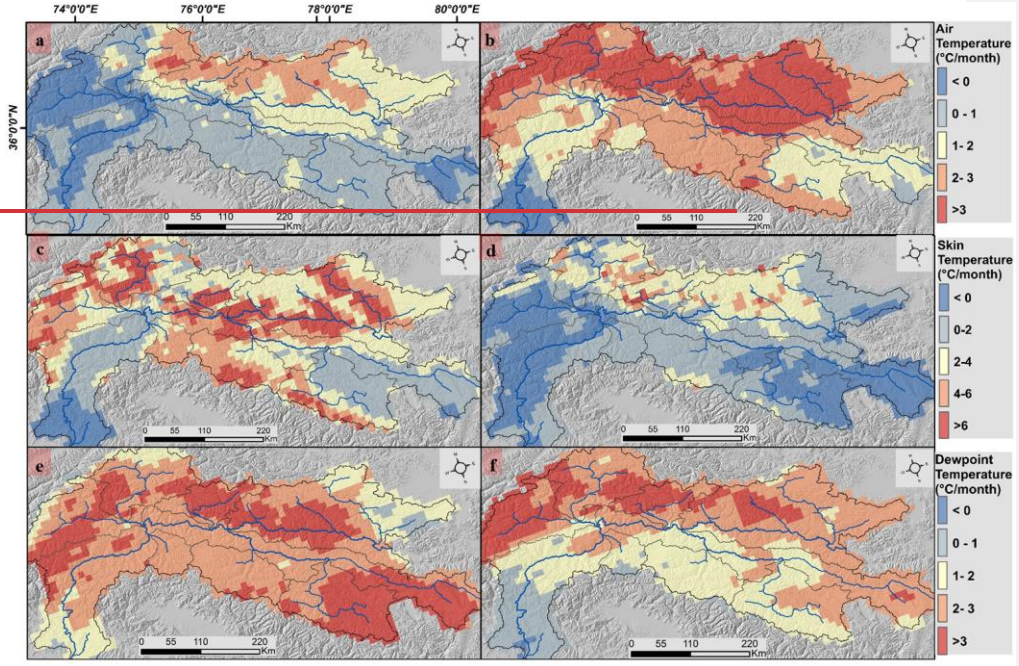
74°0'0"E
76°0'0"E
78°0'0"E
80°0'0"E
36°0'0"N
a
b
c
d
e
f
0 55 110 220 Km
Air Temperature (°C/month)
< 0
0 - 1
1- 2
2- 3
>3
Skin Temperature (°C/month)
< 0
0-2
2-4
4-6
>6
Dewpoint Temperature (°C/month)
< 0
0 - 1
1- 2
2- 3
>3

388

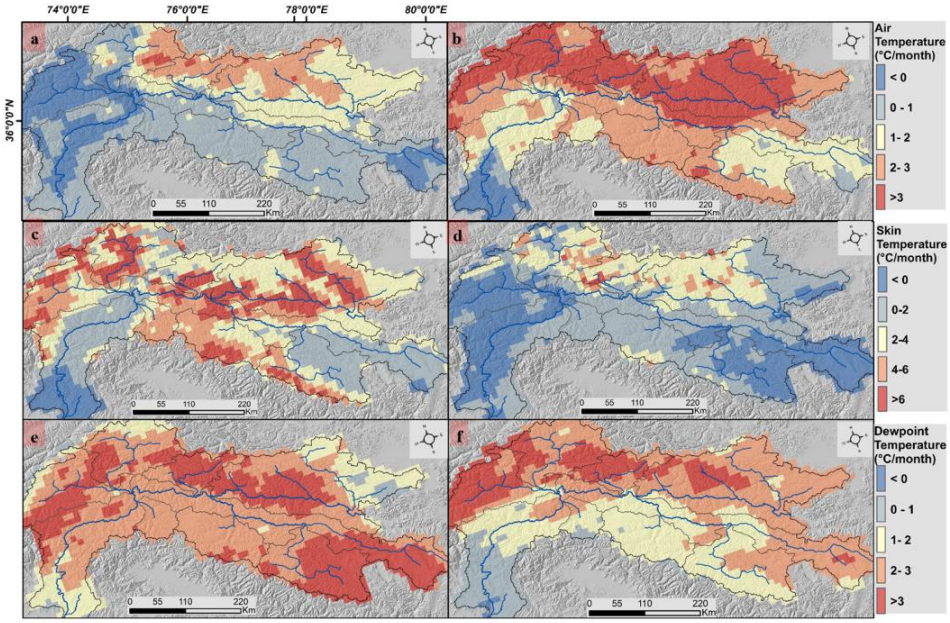

Fig. 5. Spatial distribution of hydro-meteorological variables for anomalous July and August month of 2022 across Upper Indus catchment such as: (a) Air temperature (July) (b) Air temperature (August) (c) Surface temperature (July) (d) Surface temperature (August); (e) Dewpoint temperature (July) (f) Dewpoint temperature (August).

We also observed a significant shift in the spatial distribution of change indicator variables during the observation period. In July 2022, the lower middle reaches of the Upper Indus River exhibited a negative change in EVI (~0-0.21) and a positive relative NDWI (~0.15-0.20). This inverse relationship between these two change indicators was found in the upstream channel as well in August. During the event, the tributary channels in the upstream glaciated landscape experienced a significant change in snow cover distribution, as demonstrated by the spatial variations of the relative NDSI (~ 0-0.63). Changes in relative snow cover correspond directly to increases in snowmelt and glacial runoff across glaciated catchments (Fig. 6). We observed a significant relationship ($p<0.005$; $R=0.81$) between the relative EVI metric and the anomalous stream power in the Upper Indus trunk channel and along its main tributaries. The anomalous stream power of the Upper Indus River and all of its major tributaries corresponds to a proportion

of EVI change that exceeds across low-gradient regions. This positive relationship with an increasing trend suggests a substantial geomorphic response due to extreme flooding. However, a negative relationship between anomalous stream power and EVI can also be observed across the channels of Astor and Shingo (Fig. 7).

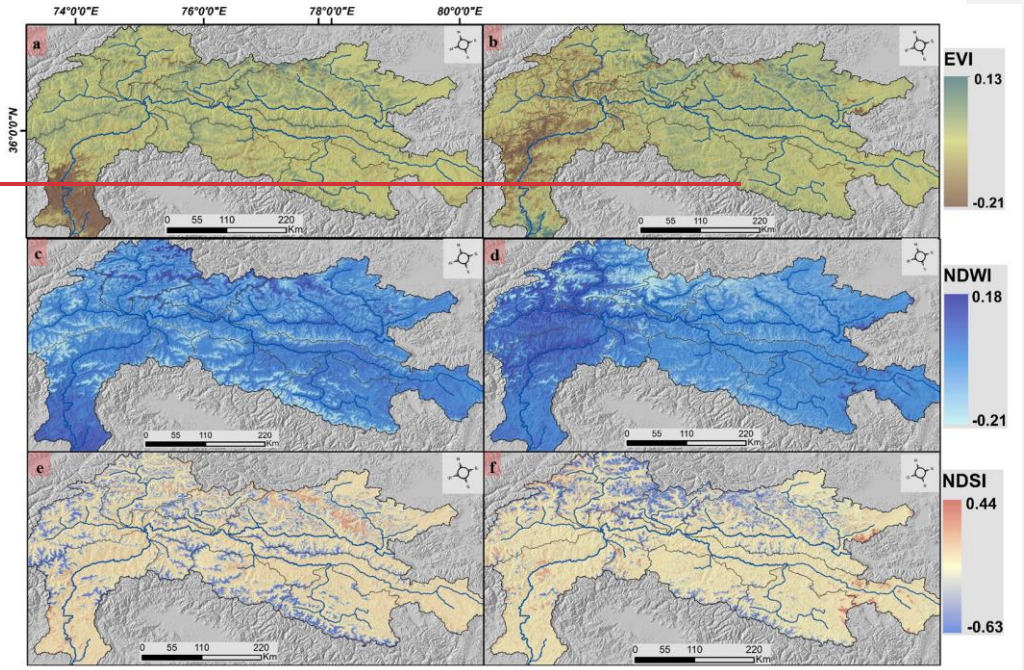

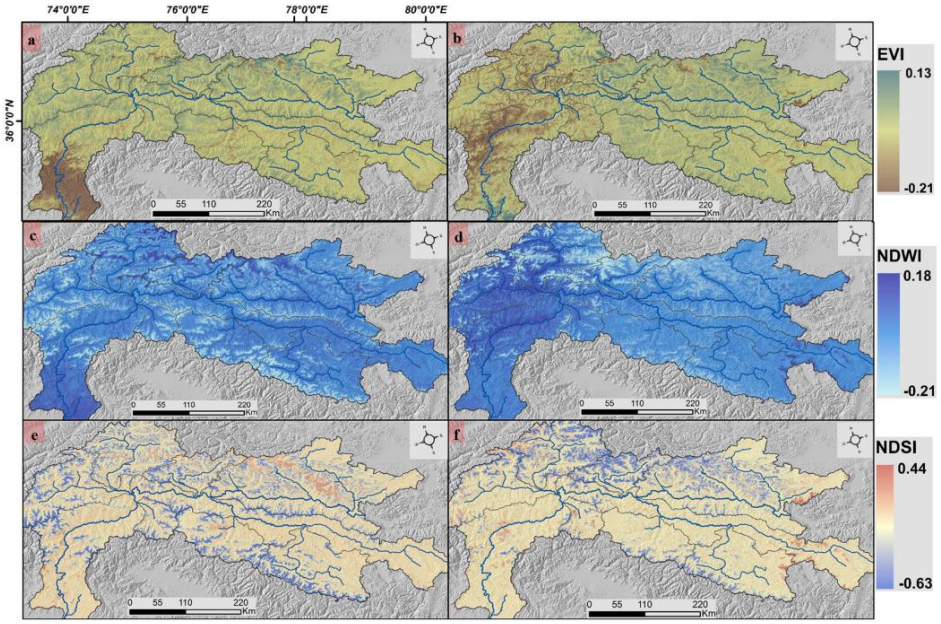

411

412 Fig. 6. Spatial distribution of hydro-meteorological variables for anomalous July and August
413 month of 2022 across Upper Indus catchment such as: (a) EVI (July) (b) EVI (August) (c) NDWI
414 (July) (d) NDWI (August); (e) NDSI (July) (f) NDSI (August).

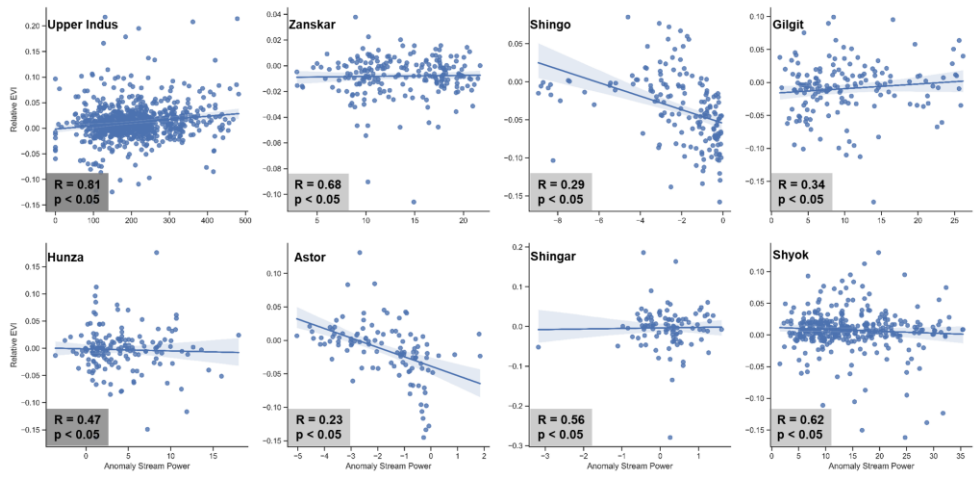

415

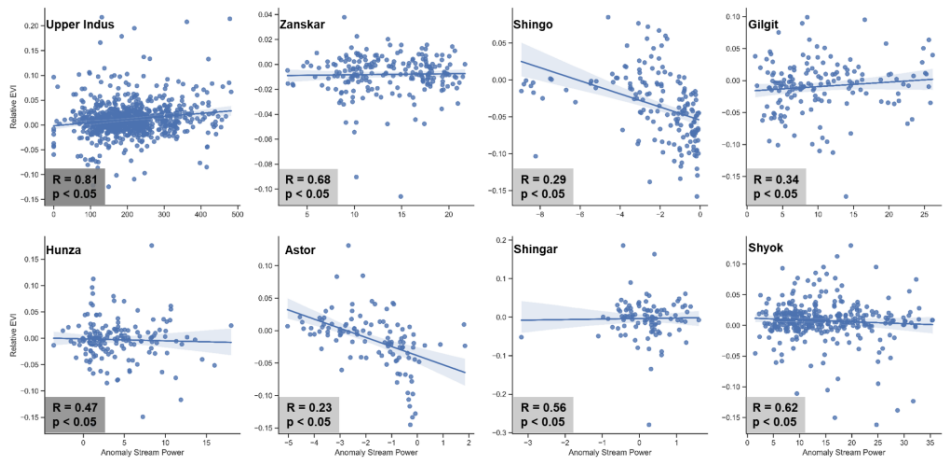

Fig.7. Statistical relationship between Relative EVI- Anomalous Stream Power from July 1 to August 31, 2022 across Upper Indus catchment as well as along its all the major tributaries.

4.3 Machine learning based approach to quantify the event anomalies

The RF-classification-based determination of variable importance indicates that dewpoint temperature is the most significant variable in estimating precipitation intensity. Other significant variables include surface temperature and air temperature. Relative NDSI was the variable of highest significance for estimating precipitation in all other sub-catchments except Shingar (Fig. S1). Snowmelt, dewpoint temperature, relative NDSI, and surface temperature are the most significant variables for each sub-catchment when estimating runoff intensity. Surface temperature holds higher significance in the trunk channel catchment of the Upper Indus, followed by air temperature and precipitation intensity (Fig. S2). The anomalous precipitation and runoff intensity are then estimated using these independent variables with the highest significance obtained during classification.

The results show that the Upper Indus catchment received significantly more precipitation and runoff than predicted at multiple instances in July and August of 2022 (Fig. 8). The anomalous and extreme characteristics of the hydro-climatic and terrestrial drivers could explain this phenomenon. The Upper Indus catchment received a significant amount of anomalous

Formatted: Font color: Auto

Formatted: Space Before: 12 pt, After: 12 pt

Formatted: Font color: Auto

precipitation, with an intensity of >~100 mm/d, which is much higher than the predicted intensity during the period of observation. The channels in the higher relief landscapes such as Astor and Gilgit encountered the second-highest anomalous incidence, with intensities ~80–100 mm/d. The upstream glaciated catchments, such as the Shyok, Shingo, and Hunza, also have persistent anomalous intensities of up to ~100 mm/d. The least impacted catchment was Zanskar and Shingo, despite a high rate of precipitation that ranges from ~60–80 mm/d.

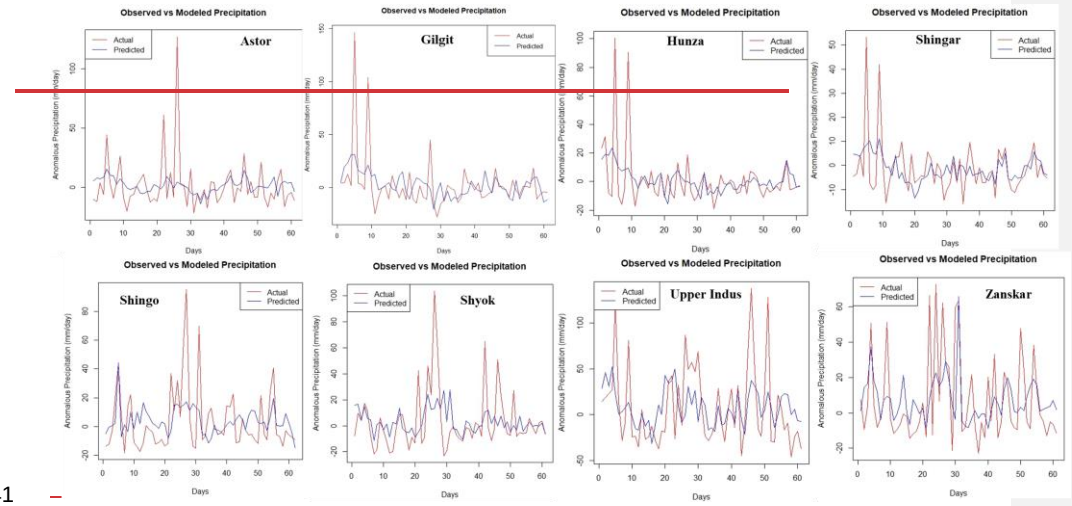

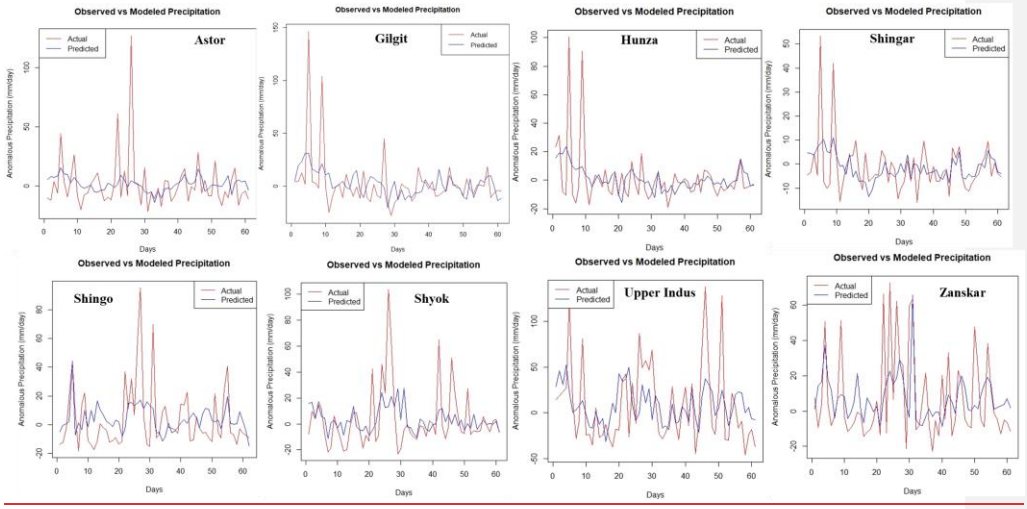

Fig. 8. Random Forest-Regression based observed vs modeled anomalous precipitation from July 1 to August 31, 2022 across Upper Indus catchment as well as along all the major tributaries.

The distribution of observed and predicted runoff shows the intensity of observed runoff corresponds with the precipitation trend. During the observation period, the Upper Indus catchment had much higher runoff rates, followed by upstream glaciated sub-catchments including Shyok (~30-60 mm/d), Shingo, and Gilgit (~20-30 mm/d). However, in the majority of the upstream sub-catchments, the observed anomalous runoff intensity is insignificant (Fig. 9).

Formatted: Font color: Auto

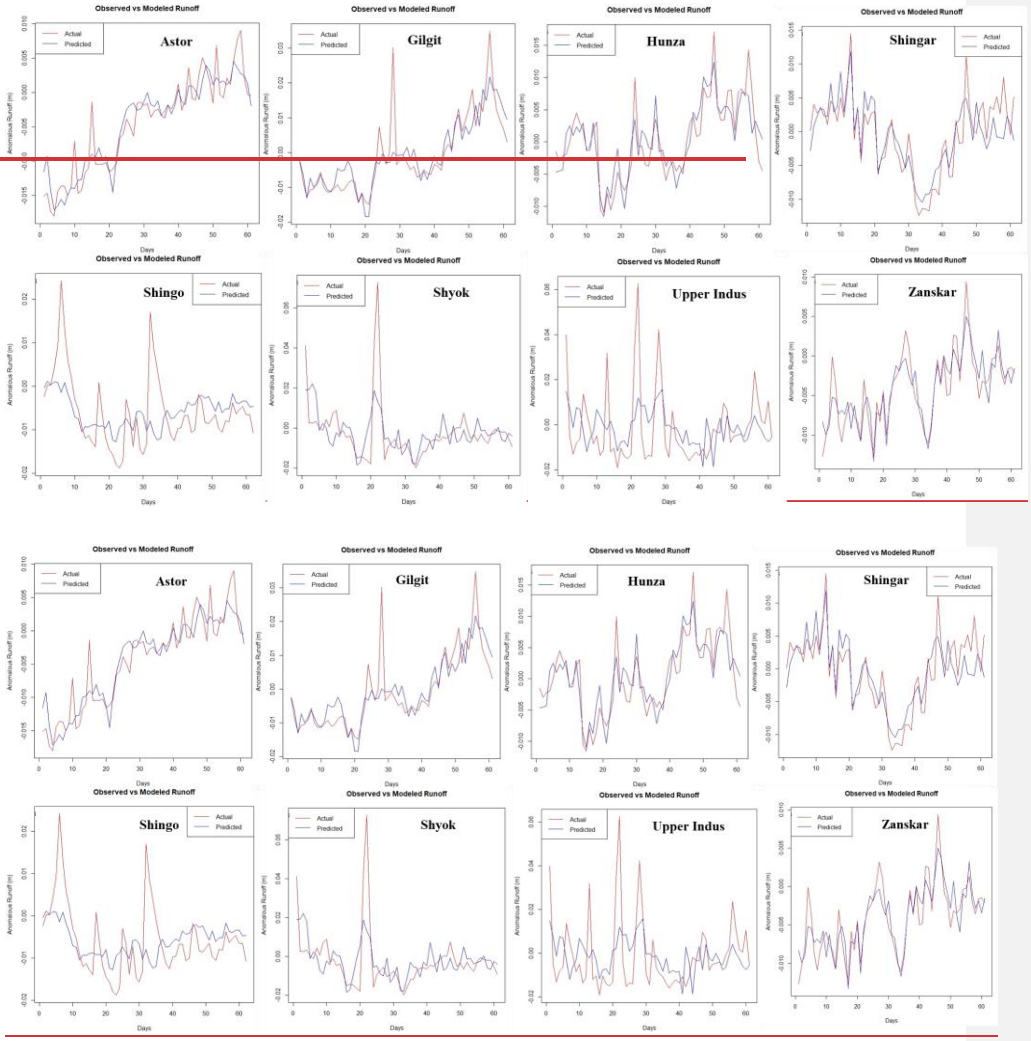

Fig. 9. Random Forest-Regression based observed vs modeled anomalous runoff from July 1 to August 31, 2022 across Upper Indus catchment as well as along all the major tributaries.

4.4 Causal relationship among Hydro-climatic variables over event duration

Formatted: Font color: Auto

Formatted: Font color: Auto

Formatted: Space Before: 12 pt, After: 12 pt

The causal analysis showed that the impact of numerous meteorological variables on the extreme flood over the Upper Indus terrain varied significantly. We observed a significant causal lagged connection between dewpoint temperature and NDSI, which together positively influenced precipitation intensity with a 1-day lag across the Upper Indus catchment. Similarly, precipitation intensity and snowmelt exhibit a positive causal influence on NDWI with a 1-day lag period. For instance, the cross-correlation between precipitation and dewpoint temperature with positive impact is > 0.4 over the event duration. There was a significant negative causal influence of NDWI on EVI, indicating an inversely proportional relationship across the observational lag period. The hydro-climatic variables such as precipitation intensity, snowmelt, NDWI, EVI, NDSI, air temperature, and surface temperature, had non-linear and non-stationary tends from July 1, 2022, to August 31, 2022, as shown by the autocorrelation and PCMCI magnitude over the time series. The auto MCI ranges of these variables are comparatively very low. Runoff and dewpoint temperatures exhibit stationarity and a linear trend over the time series with relative high auto-MCI ranges. It is also observed that dewpoint temperature has a significant inherent connection with snowmelt and NDSI, indicating that these variables have a direct causative relationship with a high cross-MCI range (Fig. 10). In a causal investigation, edges with arrows indicate a link between the drivers. However, depending on the available metrics, there may be an instant causal connection between the drivers. It should be observed that this relationship may not have been determined to be causative.

Formatted: Font color: Auto

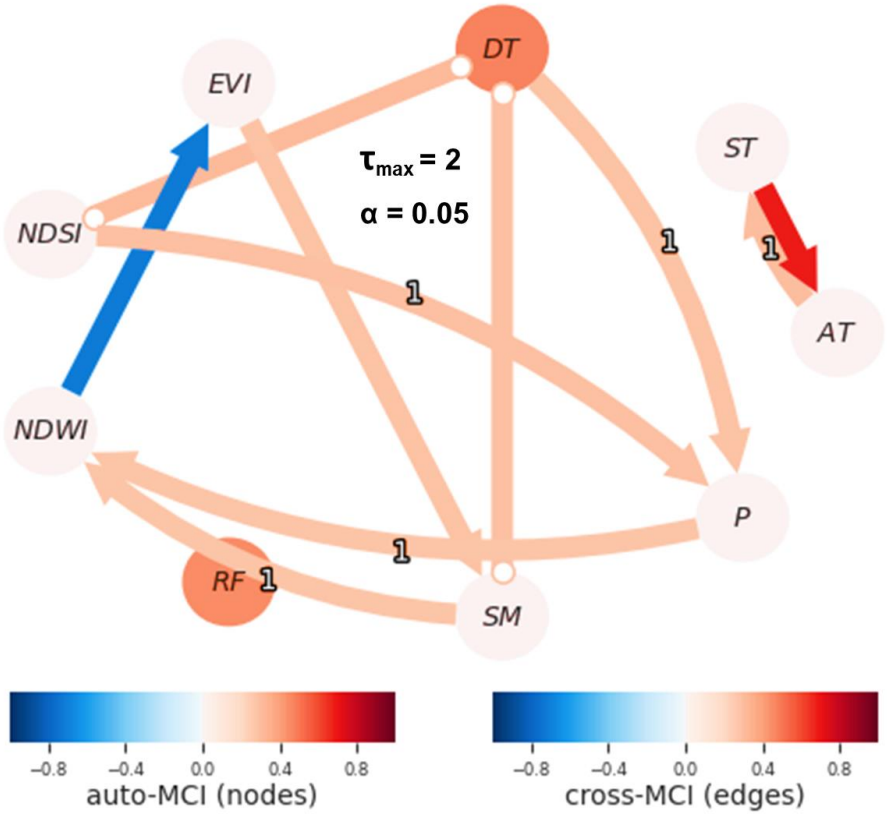

Fig.10. Causal detection among hydro-climatic driver having non-linear time series from July 1 to August 31, 2022 across Upper Indus catchment with maximum allowable lag of 2 days at the 95% CI. (The drivers are shown in the solid circles such as: DT= Dewpoint Temperature, ST= Surface Temperature, AT= Air Temperature, P= Precipitation intensity, SM= Snowmelt, RF= Runoff, NDWI= Normalized Difference Water Index, NDSI= Normalized Difference Snow Index, EVI= Enhanced Vegetation Index: The node ~~colour~~color represents autocorrelation whereas link ~~colour~~color represents the strength of directional link. The lag at which the link was found significant is shown as link label, absence of which indicates that the link was found at zero lag).

4.5 Identifying moisture trajectories for the anomalous precipitation event

Formatted: Font color: Auto

Formatted: Font color: Auto

Formatted: Font color: Auto

Formatted: Space Before: 12 pt, After: 12 pt

Based on moisture source uptake along trajectories for the observation period of July 1 to August 31, 2022, the amount of precipitation across the orographic ridges of the Upper Indus terrain was delivered along two major pathways, one from Mediterranean Sea sources such as Western disturbance (WD)-derived moisture during the onset of the monsoon and a second from the ISM, originating from the Bay of Bengal and the Arabian Sea. The WD routes provided the moisture sources for the precipitation along the 3000 m height trajectories, while the Arabian Sea, the Bay of Bengal, and the Himalayan foreland provided the moisture along the 500 m and 1000 m trajectories. Furthermore, the anomalous temperature gradient observed for the months of July and August 2022 shows that the steep bedrock valleys are causing abnormal air-mass feedback. The substantial divergence in the air-mass curve from mid-July to mid-August 2022 suggests there may have been very high precipitation and temperature fluctuations during those periods (Fig. 11).

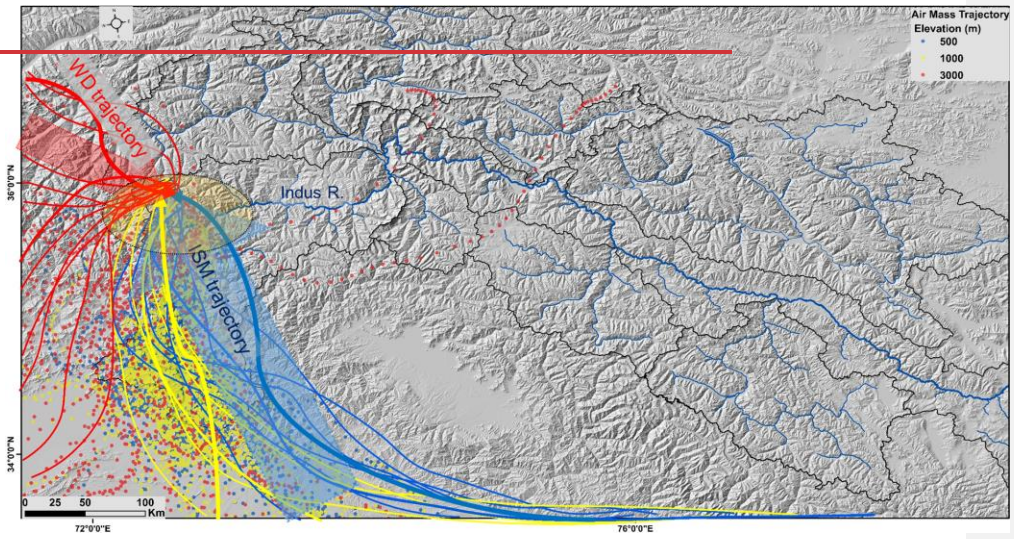

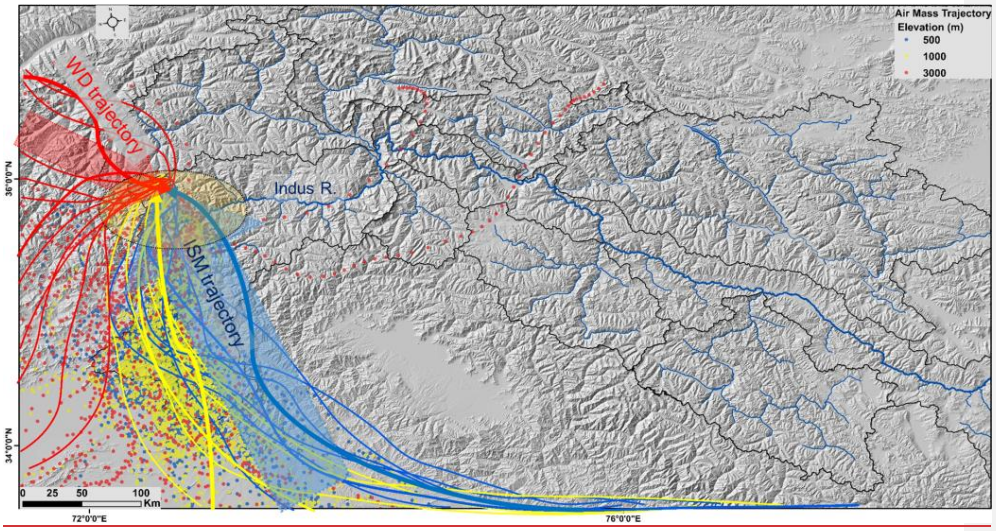

Fig.11. Moisture pathways (Backward trajectories) for Anomalous precipitation event from July 1 to August 31, 2022 across Upper Indus catchment: (Blue line denotes the trajectory of 500 m elevation, ~~Yellow~~yellow line denotes the trajectory of 1000 m elevation, and ~~Red~~red line denotes the trajectory of 3000 m elevation: Blue and yellow dot lines ~~exhibits~~exhibit the ISM pathways, whereas Red dot lines exhibit the WD pathways).

5. Discussion

Formatted: Font color: Auto

Formatted: Space Before: 12 pt, After: 12 pt

5.1 Spatial relationship between topographic metrics and event anomalies

To characterize the geomorphic response of this extreme flood, we estimated stream power over the trunk channel of the upper Indus River as an event anomaly. Understanding the spatial distribution of stream power over the longitudinal profile of bedrock rivers is essential for evaluating the catchment-scale variability in channel response to anomalous precipitation events (Whipple et al., 2000; Kaushal et al., 2020). The peaks and troughs in the stream power profile regulate the morphological characteristics of the bedrock channels (Schneider et al., 2014; Bawa et al., 2014; Sinha et al., 2017). The river morphology and channel shape will be significantly

impacted by the temporal variations in flooding intensity during anomalous precipitation events (Bookhagen and Strecker, 2012; Scherler et al., 2014).

The initial ~400–600 km length of the Upper Indus River is characterized by low gradient channels as the river traverses over the elevated-low relief landscape. After traversing through the mainstream and joining in the highest-order channel across the syntaxial region, there is a sharp rise in the stream power profile along the downstream. The western syntax (NP-HM) in the NW Himalayas is one of the most rapidly uplifting (>~5-10 mm/y) and eroding (>~10 mm/y) regions on earth, with extreme topographic relief (>3000 m) (Fig. 1; 2). The sudden increase in the stream power of the Upper Indus River after traversing through NP-HM and the resultant extreme flood along lower middle reaches were also attributed to this high elevation change (>~4000 m) and steep channel gradient (>~20-30º) (Fig. 3b). The spatial variability of stream power is also highly connected with other topographic metrics such as the k_{sn} and SL index, which demonstrate a considerable rise in their longitudinal profiles when the channel crosses the NP-HM region (Fig. 3a). We observed that the stream power distribution along the longitudinal profiles of the Upper Indus River is characterized by numerous peaks for both anomalous precipitation months in July and August 2022 (Fig. 3b).

The upstream glaciated channels of the Trans Himalayan and Karakoram ranges have a substantial glacial influence on erosion, contributing to the main trunk channel of the Upper Indus River. Therefore, such high-magnitude floods ought to propagate through the channels of high mountainous tributaries like Shyok, Gilgit, and Hunza, depending on the landscape characteristics of the upper Indus catchment. A moderate change in the distribution pattern of snow cover may have a significant impact on glacial runoff and substantially contribute to fluvial discharge. In addition to the southern mountain front, the headwaters and syntaxial zone of the Upper Indus catchment received a significant amount of precipitation, which contributed to the anomalous rise in stream power and substantially contributed to this extreme flood that influenced the channel geometry of the lower middle reach and drove high bedrock erosion (Fig. 4). However, the lower middle reaches with higher stream power are distinguished by the steep channel valley and absence of sediment deposition. The observation suggests that the higher-order channels of the Upper Indus River traversing across higher relief and steep gradient valleys likely possess direct first-order

control over the pattern of erosion when combined with an anomalous rate of precipitation (Fig. 3b).

5.2 Hydrological extremes and causal connections

Our observations suggest that the interaction of glacial runoff with fluvial discharge over the steep gradient channels combined to drive the extreme flood event across the Upper Indus catchment. These extreme hydrological episodes imply that the possible response of atmospheric instabilities may be elevation-dependent (Dimri et al., 2015; Forsythe et al., 2017; Ullah et al., 2021; Sharma et al., 2021). It commenced with anomalous rises in temperature gradients over the glaciated sub-catchments of the Upper Indus terrain, which drove the rapid changes in snow cover distribution (Fig. 5; 6). This directly impacts glacial runoff magnitude and contributes to an anomalous rise in fluvial stream power when traversed downstream over higher-relief fluvial reaches (Fig. 6). ~~The lower reaches of the Upper Indus catchment witnessed an anomalous amount of precipitation intensity from early July to late August 2022 (Fig. 4).~~The lower middle reaches of the Upper Indus catchment witnessed an anomalous amount of precipitation intensity from early July to late August 2022 (Fig. 4). When compared to the annual mean climatology, the precipitation intensity in the lower middle reaches of the Upper Indus River was roughly ~150–200% higher in the 2022 monsoon period. The 2022 Upper Indus flood represents an abrupt change from the region's prior precipitation and runoff patterns. To study this anomaly, we utilized a Random Forest model trained on climatological data from the last 40 years (1982-2021), with an emphasis on the months of July and August. The model used previous climatology as a training dataset to estimate precipitation and runoff, which are significant drivers of flooding. Despite the Random Forest model's resilience, the results revealed a substantial difference between the model's predictions and the actual observed data obtained from the 2022 flood event. The model, based on 40 years of past data, failed to capture the high precipitation and runoff patterns observed in July and August 2022 (Fig. 8: 9). The model's inability to predict rainfall intensity, as well as subsequent runoff, highlights the anomalous nature of the event. This disparity demonstrates that the 2022 flood was not only unusual but also went outside the typical climatological shifts observed over the previous four decades. This emphasizes the necessity for future modeling efforts to include other predictors, such as changes in snowmelt dynamics, atmospheric circulation anomalies, and other non-stationary phenomena.

Formatted: Space Before: 12 pt, After: 12 pt

~~When compared to the annual mean climatology, the precipitation intensity in the lower reaches of the Upper Indus River was roughly ~150–200% higher in the 2022 monsoon period.~~ The moisture flux trajectories observed during the 2022 monsoonal period across the lower middle reaches of the upper Indus River reveal two distinct sources of moisture pathways, indicating that the combined effect of the westerlies-driven precipitation and the active monsoon phase has likely caused this episodic event (Wang et al., 2017) (Fig. 11). Over the past years, the interactions between moisture-laden ISM and southward-penetrating upper-level WD depression have been linked to some catastrophic western Himalayan floods, such as in 2010 across Pakistan and 2013 in Uttarakhand, India (Rasmussen and Houze, 2012; Vellore et al., 2015; Dimri et al., 2016; Sharma et al., 2017). This anomalous rise in the rate of precipitation intensity contributes to the rapid increase in stream power across steep valleys. The combined causal influence of temperature and precipitation intensity with topography plays an important role in modulating such episodic events, as these variables eventually regulate the amount of solid precipitation, influence the change in snow cover, and have a significant impact on snowmelt runoff (Fig. 10) (Bovy et al., 2016; Godard and Tucker, 2021; Delaney et al., 2023). This flood indicates the importance of understanding the cause-and-effect relationship between temperature and precipitation in high-elevation uplands.

5.3 Channel Response to an Extreme Flood

Formatted: Font: Bold

Formatted: Space Before: 12 pt, After: 12 pt, Line spacing: Multiple 1.15 li

This study used the EVI change analysis as a significant event characteristic to capture the changes in the channel morphology triggered by the 2022 Upper Indus flood. The anomalous runoff events during the flood significantly altered channel geometry, and these changes were reflected in the spatial and temporal variations of EVI (Fig. 6). Geomorphic processes such as inundation, erosion, and landsliding have submerged or removed vegetation in areas marked by drastic shifts in EVI ranges (Anderson and Goulden, 2011). The reduction in EVI ranges along the steep channels highlights the expansion of water bodies during flooding, while the surrounding areas experienced erosion and landslides due to the extreme discharge. The broader geomorphic consequences of extreme hydrological events, such as river channel widening, sediment deposition, and riverbank erosion, frequently link to these changes in vegetation cover (Olen et al., 2016; Starke et al., 2020; Clift and Jonell, 2021; Scheip and Wegmann, 2021). While EVI cannot directly measure hydrologic parameters, its ability to reflect the loss of vegetation makes it a useful

proxy for assessing the intensity of geomorphic processes during floods. This capability is particularly important in high-mountain landscapes such as the Upper Indus, where steep landscapes and glacial fluvial regimes amplify the effects of extreme events.

We utilize NDWI and EVI as change indicator metrics to understand the changes in channel morphology due to this extreme flood event. The spatial variability of EVI corresponds significantly with an increase in NDWI intensity downstream during July and August 2022 (Fig. 6). ~~This is because increasing precipitation serves a vital role in regulating relative change in the EVI by decreasing surface albedo and temperature (Anderson and Goulden, 2011). In some cases, correlation is due to directing flooding in vegetated areas.~~

The substantial decrease in EVI values along downstream channels has also been attributed to the anomalous precipitation event, which led to increased surface runoff, higher NDWI limits, and subsequent flood deposits. We observed a significant direct causal influence with one-day-lagged connection of precipitation and snowmelt on NDWI (Fig. 10). This combined causal relationship between precipitation and snowmelt with NDWI intensity indicates that anomalous runoff occurred across both glacial and fluvial channels. Further the inverse causal connection (negative MCI ranges) between NDWI and EVI illustrates the rapid change in the channel geometry due to increase in the fluvial discharge over lower middle reaches (Fig. 10).

The change in river morphology driven by the high-magnitude flood episodes is also documented by the statistically significant ($p<0.005$; $R= 0.81$) relationship observed between anomalous stream power and relative EVI across the lower middle reaches of the Upper Indus River (Fig. 7). It is generally assumed that relative vegetation intensity is an indicator of geomorphic change that results from short-duration, high-magnitude hydrological events (Olen et al., 2016; Starke et al., 2020; Clift and Jonell, 2021; Scheip and Wegmann, 2021). Thus, we anticipate that EVI acts as a spatial indicator of change in the channel morphology across the lower middle reaches of the trunk channel during the monsoon period of 2022 (Fig. 7) suggesting that the distribution of event characteristics such as NDWI and EVI can be useful to detect the relative change in channel morphology triggered by high-magnitude floods.

Formatted: Font color: Auto

Formatted: Font color: Auto

Formatted: Space Before: 12 pt, After: 12 pt

Formatted: Font color: Auto

Formatted: Font color: Auto

Formatted: Font color: Auto

Formatted: Font color: Auto

Formatted: Font color: Auto

6. Conclusion

Formatted: Space Before: 12 pt, After: 12 pt

Our study reveals several significant event characteristics of the 2022 Upper Indus flood. Our analysis shows that the Upper Indus flood originated across elevated glacial channels due to the anomalous temperature rise, which increased the glacial runoff. This increase in runoff across glaciated catchments after traversing through fluvial reaches enhanced the fluvial discharge and likely increased the stream power in the anomalous precipitation region. The synoptic observation of moisture pathways indicates that this anomalous precipitation incident is linked to the interaction of southward moving mid-latitude westerlies troughs and eastward advancing southwestern monsoon circulation. We observe a statistically significant relationship between the anomalous stream power and relative EVI change across the lower middle reaches, which serves as a significant geomorphic indicator of change in the channel morphology. This will aid in determining the reliability of EVI as a consistent indicator of geomorphic changes, as well as its applicability in studying the geomorphic evolution of regional landscapes. This extreme flood illustrates how causal connections between temperature and precipitation across high relief-gradient channels can magnify the impacts. Such hydrological events may play significant roles as efficient geomorphic agents of erosion and, therefore, in the coupling of climatic extremes, topography, and erosion. This study underscores the susceptibility of the elevated syntaxial region to short-lived, high-magnitude flooding, indicating the need for additional research to determine the causal relationship between the drivers of hydrological extremes. Significant research is needed to understand the long-term impact of these extreme climatic events on the geomorphic processes in the region.

Formatted: Font: 12 pt, Not Bold

Code and data availability:

The Data used and methodology section includes all of the open-source datasets and tools used in the study.

Author contribution:

Abhishek ~~kashyap~~Kashyap (AK): Conceptualization, Formal analysis, Methodology, writing – original draft, Writing – review & editing.

Kristen L. Cook (KLC): Supervision, Visualization, Writing – review & editing

Mukunda Dev Behera (MDB): Supervision, Validation.

*Competing interests

The authors declare that they have no known competing financial interests or personal relationships that could have appeared to influence the work reported in this paper. We wish to confirm that there are no known conflicts of interest associated with this publication and there has been no significant financial support for this work that could have influenced its outcome.

Acknowledgments: The authors acknowledge the authorities of IIT Kharagpur for facilitating the study. AK thanks the Ministry of Education, Government of India, for the grant of a Ph.D. Research Fellowship. AK thanks the IRD "South North Scheme" scholarship, managed by Campus France, for the mobility and facilitation of a major part of this study at ISTerre, Université Grenoble Alpes.

Formatted: Default Paragraph Font, Font: Arial, 11 pt, Font color: Auto, Pattern: Clear, Highlight

Formatted: Space Before: 12 pt, After: 12 pt

Formatted: Default Paragraph Font, Font: Arial, 11 pt, Font color: Auto, Pattern: Clear, Highlight

Formatted: Default Paragraph Font, Font: Arial, 11 pt, Font color: Auto, Pattern: Clear, Highlight

Formatted: Font: 12 pt

Formatted: Default Paragraph Font, Font: Arial, 11 pt, Font color: Auto, Pattern: Clear, Highlight

Formatted: Font color: Auto, Pattern: Clear, Highlight

Formatted: Font color: Auto

7. References

Adams, B.A., Whipple, K.X., Forte, A.M., Heimsath, A.M., Hodges, K.V., 2020. Climate controls on erosion in tectonically active landscapes. Sci. Adv. 6, eaaz3166. ~~https://doi.org/10.1126/sciadv.aaz3166~~. https://doi.org/10.1126/sciadv.aaz3166

Anderson, R.G., Goulden, M.L., 2011. Relationships between climate, vegetation, and energy exchange across a montane gradient. J. Geophys. Res. 116, G01026. ~~https://doi.org/10.1029/2010JG001476~~. https://doi.org/10.1029/2010JG001476

Archer, D., 2004. Hydrological implications of spatial and altitudinal variation in temperature in the upper Indus basin. Hydrology Research 35, 209–222. ~~https://doi.org/10.2166/nh.2004.0015~~. https://doi.org/10.2166/nh.2004.0015

Bai, L., Shi, C., Li, L., Yang, Y. and Wu, J., 2018. Accuracy of CHIRPS satellite-rainfall products over mainland China. *Remote Sensing*, *10*(3), p.362. **https://doi.org/10.3390/rs10030362**

Bawa, N., Jain, V., Shekhar, S., Kumar, N., Jyani, V., 2014. Controls on morphological variability and role of stream power distribution pattern, Yamuna River, western India. Geomorphology 227, 60–72. ~~https://doi.org/10.1016/j.geomorph.2014.05.016~~. https://doi.org/10.1016/j.geomorph.2014.05.016

Formatted: Font: 12 pt, Not Bold

Formatted: Left, Space Before: 12 pt, After: 12 pt, Line spacing: Multiple 1.15 li

Formatted: Space Before: 12 pt, After: 12 pt

Formatted: Indent: Left: 1.27 cm, Widow/Orphan control, Adjust space between Latin and Asian text, Adjust space between Asian text and numbers

Formatted: Underline, Font color: Custom Color(RGB(17,85,204))

Formatted: Underline, Font color: Custom Color(RGB(17,85,204))

Formatted: Underline, Font color: Custom Color(RGB(17,85,204))

Formatted: Indent: Left: 1.27 cm, Widow/Orphan control, Adjust space between Latin and Asian text, Adjust space between Asian text and numbers

Formatted: Underline, Font color: Custom Color(RGB(17,85,204))

Benito, G., Macklin, M.G., Panin, A., Rossato, S., Fontana, A., Jones, A.F., Machado, M.J., Matlakhova, E., Mozzi, P., Zielhofer, C., 2015. Recurring flood distribution patterns related to short-term Holocene climatic variability. Sci Rep 5, 16398. https://doi.org/10.1038/srep16398. https://doi.org/10.1038/srep16398

Bhutto, F., 2022. The west is ignoring Pakistan's super-floods. Heed this warning: tomorrow it will be you. The Guardian.

Bookhagen, B., Burbank, D.W., 2006. Topography, relief, and TRMM-derived rainfall variations along the Himalaya. Geophysical Research Letters 33, 2006GL026037. https://doi.org/10.1029/2006GL026037

Bookhagen, B., Burbank, D.W., 2010. Toward a complete Himalayan hydrological budget: Spatiotemporal distribution of snowmelt and rainfall and their impact on river discharge. J. Geophys. Res. 115, 2009JF001426. https://doi.org/10.1029/2009JF001426. https://doi.org/10.1029/2009JF001426

Bookhagen, B., Burbank, D.W., 2006. Topography, relief, and TRMM-derived rainfall variations along the Himalaya. Geophysical Research Letters 33, 2006GL026037. https://doi.org/10.1029/2006GL026037

Bookhagen, B., Strecker, M.R., 2012. Spatiotemporal trends in erosion rates across a pronounced rainfall gradient: Examples from the southern Central Andes. Earth and Planetary Science Letters 327–328, 97–110. https://doi.org/10.1016/j.epsl.2012.02.005. https://doi.org/10.1016/j.epsl.2012.02.005

Bookhagen, B., Thiede, R.C., Strecker, M.R., 2005a. Abnormal monsoon years and their control on erosion and sediment flux in the high, arid northwest Himalaya. Earth and Planetary Science Letters 231, 131–146. https://doi.org/10.1016/j.epsl.2004.11.014. https://doi.org/10.1016/j.epsl.2004.11.014

Bookhagen, B., Thiede, R.C., Strecker, M.R., 2005b. Late Quaternary intensified monsoon phases control landscape evolution in the northwest Himalaya. Geol 33, 149. https://doi.org/10.1130/G20982.1. https://doi.org/10.1130/G20982.1

Bovy, B., Braun, J., Demoulin, A., 2016. A new numerical framework for simulating the control of weather and climate on the evolution of soil-mantled hillslopes.

Formatted: Underline, Font color: Custom Color(RGB(17,85,204))

Formatted: Indent: Left: 1.27 cm, Widow/Orphan control, Adjust space between Latin and Asian text, Adjust space between Asian text and numbers

Formatted: Underline, Font color: Custom Color(RGB(17,85,204))

Formatted: Indent: Left: 1.27 cm, Widow/Orphan control, Adjust space between Latin and Asian text, Adjust space between Asian text and numbers

Formatted: Underline, Font color: Custom Color(RGB(17,85,204))

Formatted: Underline, Font color: Custom Color(RGB(17,85,204))

Formatted: Underline, Font color: Custom Color(RGB(17,85,204))

Geomorphology 263, 99–112. https://doi.org/10.1016/j.geomorph.2016.03.016 . https://doi.org/10.1016/j.geomorph.2016.03.016

Breiman, L., 2001. [No title found]. Machine Learning 45, 5–32. https://doi.org/10.1023/A:1010933404324 . https://doi.org/10.1023/A:1010933404324

Burbank, D.W., Anderson, R.S., 2011. Tectonic geomorphology. John Wiley & Sons.

Butler, R.W.H., 2019. Tectonic evolution of the Himalayan syntaxes: the view from Nanga Parbat. SP 483, 215–254. https://doi.org/10.1144/SP483.5 . https://doi.org/10.1144/SP483.5

Clift, P.D., Jonell, T.N., 2021. Monsoon controls on sediment generation and transport: Mass budget and provenance constraints from the Indus River catchment, delta and submarine fan over tectonic and multimillennial timescales. Earth-Science Reviews 220, 103682. https://doi.org/10.1016/j.earscirev.2021.103682 . https://doi.org/10.1016/j.earscirev.2021.103682

Cook, K.L., Andermann, C., Gimbert, F., Adhikari, B.R., Hovius, N., 2018. Glacial lake outburst floods as drivers of fluvial erosion in the Himalaya. Science 362, 53–57. https://doi.org/10.1126/science.aat4981 . https://doi.org/10.1126/science.aat4981

Delaney, I., Anderson, L., Herman, F., 2023. Modeling the spatially distributed nature of subglacial sediment transport and erosion. Earth Surf. Dynam. 11, 663–680. https://doi.org/10.5194/esurf-11-663-2023 . https://doi.org/10.5194/esurf-11-663-2023

Dimri, A.P., Chevuturi, A., Niyogi, D., Thayyen, R.J., Ray, K., Tripathi, S.N., Pandey, A.K., Mohanty, U.C., 2017. Cloudbursts in Indian Himalayas: A review. Earth-Science Reviews 168, 1–23. https://doi.org/10.1016/j.earscirev.2017.03.006 . https://doi.org/10.1016/j.earscirev.2017.03.006

Dimri, A.P., Niyogi, D., Barros, A.P., Ridley, J., Mohanty, U.C., Yasunari, T., Sikka, D.R., 2015. Western Disturbances: A review. Reviews of Geophysics 53, 225–246. https://doi.org/10.1002/2014RG000460 . https://doi.org/10.1002/2014RG000460

Dimri, A.P., Yasunari, T., Kotlia, B.S., Mohanty, U.C., Sikka, D.R., 2016. Indian winter monsoon: Present and past. Earth-Science Reviews 163, 297–322.

Formatted: Underline, Font color: Custom Color(RGB(17,85,204))

https://doi.org/10.1016/j.earscirev.2016.10.008 . https://doi.org/10.1016/j.earscirev.2016.10.008

Fadil, A., 2022. Devastating floods in Pakistan claim lives of more than 500 children. UNICEF.

Farinotti, D., Immerzeel, W.W., De Kok, R.J., Quincey, D.J., Dehecq, A., 2020. Manifestations and mechanisms of the Karakoram glacier Anomaly. Nat. Geosci. 13, 8–16. https://doi.org/10.1038/s41561-019-0513-5 . https://doi.org/10.1038/s41561-019-0513-5

Forsythe, N., Fowler, H.J., Li, X.-F., Blenkinsop, S., Pritchard, D., 2017. Karakoram temperature and glacial melt driven by regional atmospheric circulation variability. Nature Clim Change 7, 664–670. https://doi.org/10.1038/nclimate3361. https://doi.org/10.1038/nclimate3361

Gao, F., Zhang, Y., Ren, X., Yao, Y., Hao, Z. and Cai, W., 2018. Evaluation of CHIRPS and its application for drought monitoring over the Haihe River Basin, China. Natural Hazards, 92, pp.155-172. https://doi.org/10.1007/s11069-018-3196-0

Godard, V., Bourles, D.L., Spinabella, F., Burbank, D.W., Bookhagen, B., Fisher, G.B., Moulin, A., Leanni, L., 2014. Dominance of tectonics over climate in Himalayan denudation. Geology 42, 243–246. https://doi.org/10.1130/G35342.1 . https://doi.org/10.1130/G35342.1

Godard, V., Tucker, G.E., 2021. Influence of Climate-Forcing Frequency on Hillslope Response. Geophysical Research Letters 48, e2021GL094305. https://doi.org/10.1029/2021GL094305 . https://doi.org/10.1029/2021GL094305

Goodbred, S.L., Kuehl, S.A., Steckler, M.S., Sarker, M.H., 2003. Controls on facies distribution and stratigraphic preservation in the Ganges–Brahmaputra delta sequence. Sedimentary Geology 155, 301–316. https://doi.org/10.1016/S0037-0738(02)00184-7 . https://doi.org/10.1016/S0037-0738(02)00184-7

Hack, J.T., 1973. Stream-profile analysis and stream-gradient index. Journal of Research of the us Geological Survey 1, 421–429.

Hewitt, K., 2007. Tributary glacier surges: an exceptional concentration at Panmah Glacier, Karakoram Himalaya. J. Glaciol. 53, 181–188. https://doi.org/10.3189/172756507782202829

Formatted: Underline, Font color: Custom Color(RGB(17,85,204))

Formatted: Underline, Font color: Custom Color(RGB(17,85,204))

Formatted: Indent: Left: 0 cm, First line: 0 cm, Widow/Orphan control, Adjust space between Latin and Asian text, Adjust space between Asian text and numbers

Formatted: Indent: Left: 1.27 cm, Widow/Orphan control, Adjust space between Latin and Asian text, Adjust space between Asian text and numbers

Formatted: Underline, Font color: Custom Color(RGB(17,85,204))

Formatted: Underline, Font color: Custom Color(RGB(17,85,204))

Formatted: Underline, Font color: Custom Color(RGB(17,85,204))

Hewitt, K., 2009. Catastrophic rock slope failures and late Quaternary developments in the Nanga Parbat–Haramosh Massif, Upper Indus basin, northern Pakistan. Quaternary Science Reviews 28, 1055–1069. https://doi.org/10.1016/j.quascirev.2008.12.019 . https://doi.org/10.1016/j.quascirev.2008.12.019

Hewitt, K., 2007. Tributary glacier surges: an exceptional concentration at Panmah Glacier, Karakoram Himalaya. J. Glaciol. 53, 181–188. https://doi.org/10.3189/172756507782202829

Houze, R.A., Rasmussen, K.L., Medina, S., Brodzik, S.R., Romatschke, U., 2011. Anomalous Atmospheric Events Leading to the Summer 2010 Floods in Pakistan. Bulletin of the American Meteorological Society 92, 291–298. https://doi.org/10.1175/2010BAMS3173.1 . https://doi.org/10.1175/2010BAMS3173.1

Immerzeel, W.W., Van Beek, L.P.H., Bierkens, M.F.P., 2010. Climate Change Will Affect the Asian Water Towers. Science 328, 1382–1385. https://doi.org/10.1126/science.1183188 . https://doi.org/10.1126/science.1183188

Jaiswara, N.K., Kotluri, S.K., Pandey, A.K., Pandey, P., 2019. Transient basin as indicator of tectonic expressions in bedrock landscape: Approach based on MATLAB geomorphic tool (Transient-profiler). Geomorphology 346, 106853. https://doi.org/10.1016/j.geomorph.2019.106853 . https://doi.org/10.1016/j.geomorph.2019.106853

Jaiswara, N.K., Kotluri, S.K., Pandey, P., Pandey, A.K., 2020. MATLAB functions for extracting hypsometry, stream-length gradient index, steepness index, chi gradient of channel and swath profiles from digital elevation model (DEM) and other spatial data for landscape characterisation. Applied Computing and Geosciences 7, 100033. https://doi.org/10.1016/j.acags.2020.100033 . https://doi.org/10.1016/j.acags.2020.100033

Jones, B., 2022. How melting glaciers fueled Pakistan's fatal floods.

Formatted: Indent: Left: 1.27 cm, Widow/Orphan control, Adjust space between Latin and Asian text, Adjust space between Asian text and numbers

Formatted: Underline, Font color: Custom Color(RGB(17,85,204))

Formatted: Indent: Left: 1.27 cm, Widow/Orphan control, Adjust space between Latin and Asian text, Adjust space between Asian text and numbers

Formatted: Underline, Font color: Custom Color(RGB(17,85,204))

Formatted: Underline, Font color: Custom Color(RGB(17,85,204))

Formatted: Underline, Font color: Custom Color(RGB(17,85,204))

Formatted: Underline, Font color: Custom Color(RGB(17,85,204))

Joshi, S.K., Kumar, S., Sinha, R., Rai, S.P., Khobragade, S., Rao, M.S., 2023. Identifying moisture transport pathways for north-west India. Geological Journal 58, 4428–4440. https://doi.org/10.1002/gj.4759 . https://doi.org/10.1002/gj.4759

Kapnick, S.B., Delworth, T.L., Ashfaq, M., Malyshev, S., Milly, P.C.D., 2014. Snowfall less sensitive to warming in Karakoram than in Himalayas due to a unique seasonal cycle. Nature Geosci 7, 834–840. https://doi.org/10.1038/ngeo2269 . https://doi.org/10.1038/ngeo2269

Karmouche, S., Galytska, E., Runge, J., Meehl, G.A., Phillips, A.S., Weigel, K., Eyring, V., 2023. Regime-oriented causal model evaluation of Atlantic–Pacific teleconnections in CMIP6. Earth Syst. Dynam. 14, 309–344. https://doi.org/10.5194/esd-14-309-2023 . https://doi.org/10.5194/esd-14-309-2023

Kashyap, A., Behera, M.D., 2023. The influence of landslide morphology on erosion rate variability across western Himalayan catchments: Role of westerlies and summer monsoon interaction in the landscape characterization. Geological Journal gj.4913. https://doi.org/10.1002/gj.4913 . https://doi.org/10.1002/gj.4913

Kashyap, A., Behera, M.D., Pradhan, B., 2024. Differential surface uplift and knickpoint evolution along the transient Teesta river in the eastern Himalayas. Journal of Asian Earth Sciences 260, 105974. https://doi.org/10.1016/j.jseaes.2023.105974. https://doi.org/10.1016/j.jseaes.2023.105974

Katsanos, D., Retalis, A. and Michaelides, S., 2016. Validation of a high-resolution precipitation database (CHIRPS) over Cyprus for a 30-year period. *Atmospheric Research*, *169*, pp.459-464. https://doi.org/10.1016/j.atmosres.2015.05.015

Kaushal, R.K., Sarkar, A., Mishra, K., Sinha, R., Nepal, S., Jain, V., 2020. Spatio-temporal variability in stream power distribution in the Upper Kosi River basin, Central Himalaya: Controls and geomorphic implications. Geomorphology 350, 106888. https://doi.org/10.1016/j.geomorph.2019.106888 . https://doi.org/10.1016/j.geomorph.2019.106888

Khokhar, M.N., 2022. Rich countries caused Pakistan's catastrophic flooding. Their response? Inertia and apathy. The Guardian.

Formatted: Underline, Font color: Custom Color(RGB(17,85,204))

Formatted: Underline, Font color: Custom Color(RGB(17,85,204))

Formatted: Underline, Font color: Custom Color(RGB(17,85,204))

Formatted: Underline, Font color: Custom Color(RGB(17,85,204))

Formatted: Indent: Left: 0 cm, First line: 0 cm, Widow/Orphan control, Adjust space between Latin and Asian text, Adjust space between Asian text and numbers

Formatted: Indent: Left: 1.27 cm, Widow/Orphan control, Adjust space between Latin and Asian text, Adjust space between Asian text and numbers

Formatted: Underline, Font color: Custom Color(RGB(17,85,204))

Kirby, E., Whipple, K.X., 2012. Expression of active tectonics in erosional landscapes. Journal of Structural Geology 44, 54–75. https://doi.org/10.1016/j.jsg.2012.07.009 . https://doi.org/10.1016/j.jsg.2012.07.009

Knox, J.C., 2000. Sensitivity of modern and Holocene floods to climate change. Quaternary Science Reviews 19, 439–457. https://doi.org/10.1016/S0277-3791(99)00074-8 . https://doi.org/10.1016/S0277-3791(99)00074-8

Koons, P., Zeitler, P., Chamberlain, C., Craw, D., Meltzer, A., 2002. Mechanical links between erosion and metamorphism in Nanga Parbat, Pakistan Himalaya. American Journal of Science 302, 749–773.

Koons, P.O., Zeitler, P., Hallet, B., 2013. Tectonic aneurysms and mountain building. Treatise on geomorphology 5, 318–349.

Korup, O., 2012. Earth's portfolio of extreme sediment transport events. Earth-Science Reviews 112, 115–125. https://doi.org/10.1016/j.earscirev.2012.02.006 . https://doi.org/10.1016/j.earscirev.2012.02.006

Korup, O., Densmore, A.L., Schlunegger, F., 2010a. The role of landslides in mountain range evolution. Geomorphology 120, 77–90. https://doi.org/10.1016/j.geomorph.2009.09.017 . https://doi.org/10.1016/j.geomorph.2009.09.017

Korup, O., Montgomery, D.R., 2008. Tibetan plateau river incision inhibited by glacial stabilization of the Tsangpo gorge. Nature 455, 786–789. https://doi.org/10.1038/nature07322 . https://doi.org/10.1038/nature07322

Korup, O., Montgomery, D.R., Hewitt, K., 2010b. Glacier and landslide feedbacks to topographic relief in the Himalayan syntaxes. Proc. Natl. Acad. Sci. U.S.A. 107, 5317–5322. https://doi.org/10.1073/pnas.0907531107 . https://doi.org/10.1073/pnas.0907531107

Kretschmer, M., Runge, J., Coumou, D., 2017. Early prediction of extreme stratospheric polar vortex states based on causal precursors. Geophysical Research Letters 44, 8592–8600. https://doi.org/10.1002/2017GL074696 . https://doi.org/10.1002/2017GL074696

Formatted: Underline, Font color: Custom Color(RGB(17,85,204))

Formatted: Underline, Font color: Custom Color(RGB(17,85,204))

Formatted: Underline, Font color: Custom Color(RGB(17,85,204))

Formatted: Underline, Font color: Custom Color(RGB(17,85,204))

Formatted: Underline, Font color: Custom Color(RGB(17,85,204))

Formatted: Underline, Font color: Custom Color(RGB(17,85,204))

Formatted: Underline, Font color: Custom Color(RGB(17,85,204))

Krich, C., Runge, J., Miralles, D.G., Migliavacca, M., Perez-Priego, O., El-Madany, T., Carrara, A., Mahecha, M.D., 2020. Estimating causal networks in biosphere–atmosphere interaction with the PCMCI approach. Biogeosciences 17, 1033–1061. https://doi.org/10.5194/bg-17-1033-2020 . https://doi.org/10.5194/bg-17-1033-2020

Lague, D., 2014. The stream power river incision model: evidence, theory and beyond. Earth Surf Processes Landf 39, 38–61. https://doi.org/10.1002/esp.3462 . https://doi.org/10.1002/esp.3462

Leland, J., Reid, M.R., Burbank, D.W., Finkel, R., Caffee, M., 1998. Incision and differential bedrock uplift along the Indus River near Nanga Parbat, Pakistan Himalaya, from 10Be and 26Al exposure age dating of bedrock straths. Earth and Planetary Science Letters 154, 93–107. https://doi.org/10.1016/S0012-821X(97)00171-4 . https://doi.org/10.1016/S0012-821X(97)00171-4

Leonard, J.S., Whipple, K.X., Heimsath, A.M., 2023a. Controls on topography and erosion of the north-central Andes. Geology. https://doi.org/10.1130/G51618.1 . https://doi.org/10.1130/G51618.1

Leonard, J.S., Whipple, K.X., Heimsath, A.M., 2023b. Isolating climatic, tectonic, and lithologic controls on mountain landscape evolution. Sci. Adv. 9, eadd8915. https://doi.org/10.1126/sciadv.add8915 . https://doi.org/10.1126/sciadv.add8915

Liu, P., Li, L., Guo, S., Xiong, L., Zhang, W., Zhang, J., Xu, C.-Y., 2015. Optimal design of seasonal flood limited water levels and its application for the Three Gorges Reservoir. Journal of Hydrology 527, 1045–1053. https://doi.org/10.1016/j.jhydrol.2015.05.055 . https://doi.org/10.1016/j.jhydrol.2015.05.055

Ma, Y., Hu, X., Chen, Y., Hu, Z., Feng, T., Feng, G., 2023. Different Characteristics and Drivers of the Extraordinary Pakistan Rainfall in July and August 2022. Remote Sensing 15, 2311. https://doi.org/10.3390/rs15092311 . https://doi.org/10.3390/rs15092311

Montgomery, D.R., Balco, G., Willett, S.D., 2001. Climate, tectonics, and the morphology of the Andes. Geol 29, 579. https://doi.org/10.1130/0091-7613(2001)029<0579: CTATMO>2.0.CO;2

Formatted: Underline, Font color: Custom Color(RGB(17,85,204))

Formatted: Underline, Font color: Custom Color(RGB(17,85,204))

Formatted: Underline, Font color: Custom Color(RGB(17,85,204))

Formatted: Underline, Font color: Custom Color(RGB(17,85,204))

Formatted: Underline, Font color: Custom Color(RGB(17,85,204))

Formatted: Underline, Font color: Custom Color(RGB(17,85,204))

Formatted: Underline, Font color: Custom Color(RGB(17,85,204))

Nanditha, J.S., Kushwaha, A.P., Singh, R., Malik, I., Solanki, H., Chuphal, D.S., Dangar, S., Mahto, S.S., Vegad, U., Mishra, V., 2023. The Pakistan Flood of August 2022: Causes and Implications. Earth's Future 11, e2022EF003230. https://doi.org/10.1029/2022EF003230. https://doi.org/10.1029/2022EF003230

Nawaz, M., Iqbal, M.F. and Mahmood, I., 2021. Validation of CHIRPS satellite-based precipitation dataset over Pakistan. *Atmospheric Research*, *248*, p.105289. https://doi.org/10.1016/j.atmosres.2020.105289

NDMA, 2022. NDMA monsoon 2022 daily situation report No 093.

Nowack, P., Runge, J., Eyring, V., Haigh, J.D., 2020. Causal networks for climate model evaluation and constrained projections. Nat Commun 11, 1415. https://doi.org/10.1038/s41467-020-15195-y. https://doi.org/10.1038/s41467-020-15195-y

Olen, S.M., Bookhagen, B., Strecker, M.R., 2016. Role of climate and vegetation density in modulating denudation rates in the Himalaya. Earth and Planetary Science Letters 445, 57–67. https://doi.org/10.1016/j.epsl.2016.03.047. https://doi.org/10.1016/j.epsl.2016.03.047

Otto, F.E.L., Zachariah, M., Saeed, F., Siddiqi, A., Kamil, S., Mushtaq, H., Arulalan, T., AchutaRao, K., Chaithra, S.T., Barnes, C., Philip, S., Kew, S., Vautard, R., Koren, G., Pinto, I., Wolski, P., Vahlberg, M., Singh, R., Arrighi, J., Van Aalst, M., Thalheimer, L., Raju, E., Li, S., Yang, W., Harrington, L.J., Clarke, B., 2023. Climate change increased extreme monsoon rainfall, flooding highly vulnerable communities in Pakistan. Environ. Res.: Climate 2, 025001. https://doi.org/10.1088/2752-5295/acbfd5. https://doi.org/10.1088/2752-5295/acbfd5

Panda, S., Kumar, A., Das, S., Devrani, R., Rai, S., Prakash, K., Srivastava, P., 2020. Chronology and sediment provenance of extreme floods of Siang River (Tsangpo-Brahmaputra River valley), northeast Himalaya. Earth Surf Processes Landf 45, 2495–2511. https://doi.org/10.1002/esp.4893. https://doi.org/10.1002/esp.4893

Paredes-Trejo, F.J., Barbosa, H.A. and Kumar, T.L., 2017. Validating CHIRPS-based satellite precipitation estimates in Northeast Brazil. *Journal of arid environments*, *139*, pp.26-40. https://doi.org/10.1016/j.jaridenv.2016.12.009

Formatted: Indent: Left: 0 cm, First line: 0 cm, Widow/Orphan control, Adjust space between Latin and Asian text, Adjust space between Asian text and numbers

Formatted: Indent: Left: 1.27 cm, Widow/Orphan control, Adjust space between Latin and Asian text, Adjust space between Asian text and numbers

Formatted: Underline, Font color: Custom Color(RGB(17,85,204))

Formatted: Underline, Font color: Custom Color(RGB(17,85,204))

Formatted: Underline, Font color: Custom Color(RGB(17,85,204))

Formatted: Underline, Font color: Custom Color(RGB(17,85,204))

Piatrunia, N., 0000-0002-5341-7964, 2022. Glacial to Holocene climate variability in the southern mid latitudes. https://doi.org/10.26153/TSW/45137 . https://doi.org/10.26153/TSW/45137

Rasmussen, K.L., Houze, R.A., 2012. A Flash-Flooding Storm at the Steep Edge of High Terrain: Disaster in the Himalayas. Bulletin of the American Meteorological Society 93, 1713–1724. https://doi.org/10.1175/BAMS-D-11-00236.1 . https://doi.org/10.1175/BAMS-D-11-00236.1

Ray, K., Pandey, P., Pandey, C., Dimri, A., Kishore, K., 2019. On the recent floods in India. Current science 117, 204–218.

Rossi, M.W., Whipple, K.X., Vivoni, E.R., 2016. Precipitation and evapotranspiration controls on daily runoff variability in the contiguous United States and Puerto Rico. JGR Earth Surface 121, 128–145. https://doi.org/10.1002/2015JF003446 . https://doi.org/10.1002/2015JF003446

Runge, J., 2018. Causal network reconstruction from time series: From theoretical assumptions to practical estimation. Chaos: An Interdisciplinary Journal of Nonlinear Science 28, 075310. https://doi.org/10.1063/1.5025050 . https://doi.org/10.1063/1.5025050

Runge, J., Bathiany, S., Bollt, E., Camps-Valls, G., Coumou, D., Deyle, E., Glymour, C., Kretschmer, M., Mahecha, M.D., Muñoz-Marí, J., Van Nes, E.H., Peters, J., Quax, R., Reichstein, M., Scheffer, M., Schölkopf, B., Spirtes, P., Sugihara, G., Sun, J., Zhang, K., Zscheischler, J., 2019a. Inferring causation from time series in Earth system sciences. Nat Commun 10, 2553. https://doi.org/10.1038/s41467-019-10105-3 . https://doi.org/10.1038/s41467-019-10105-3

Runge, J., Gao, P., Garcin, F., Faltings, B., 2014. Churn prediction for high-value players in casual social games, in: 2014 IEEE Conference on Computational Intelligence and Games. Presented at the 2014 IEEE Conference on Computational Intelligence and Games (CIG), IEEE, Dortmund, Germany, pp. 1–8. https://doi.org/10.1109/CIG.2014.6932875 . https://doi.org/10.1109/CIG.2014.6932875

Runge, J., Gerhardus, A., Varando, G., Eyring, V., Camps-Valls, G., 2023. Causal inference for time series. Nat Rev Earth Environ 4, 487–505.

Formatted: Indent: Left: 1.27 cm, Widow/Orphan control, Adjust space between Latin and Asian text, Adjust space between Asian text and numbers

Formatted: Underline, Font color: Custom Color(RGB(17,85,204))

Formatted: Underline, Font color: Custom Color(RGB(17,85,204))

Formatted: Underline, Font color: Custom Color(RGB(17,85,204))

Formatted: Underline, Font color: Custom Color(RGB(17,85,204))

Formatted: Underline, Font color: Custom Color(RGB(17,85,204))

Formatted: Underline, Font color: Custom Color(RGB(17,85,204))

https://doi.org/10.1038/s43017-023-00431-y . https://doi.org/10.1038/s43017-023-00431-y

Runge, J., Nowack, P., Kretschmer, M., Flaxman, S., Sejdinovic, D., 2019b. Detecting and quantifying causal associations in large nonlinear time series datasets. Sci. Adv. 5, eaau4996. https://doi.org/10.1126/sciadv.aau4996 . https://doi.org/10.1126/sciadv.aau4996

Scheip, C.M., Wegmann, K.W., 2021. HazMapper: a global open-source natural hazard mapping application in Google Earth Engine. Nat. Hazards Earth Syst. Sci. 21, 1495–1511. https://doi.org/10.5194/nhess-21-1495-2021 . https://doi.org/10.5194/nhess-21-1495-2021

Scherler, D., Bookhagen, B., Strecker, M.R., 2011. Spatially variable response of Himalayan glaciers to climate change affected by debris cover. Nature Geosci 4, 156–159. https://doi.org/10.1038/ngeo1068 . https://doi.org/10.1038/ngeo1068

Schneider, J.M., Turowski, J.M., Rickenmann, D., Hegglin, R., Arrigo, S., Mao, L., Kirchner, J.W., 2014. Scaling relationships between bed load volumes, transport distances, and stream power in steep mountain channels: Tracer Erlenbach. J. Geophys. Res. Earth Surf. 119, 533–549. https://doi.org/10.1002/2013JF002874 . https://doi.org/10.1002/2013JF002874

Schwanghart, W., Scherler, D., 2014. Short Communication: TopoToolbox 2 – MATLAB-based software for topographic analysis and modeling in Earth surface sciences. Earth Surf. Dynam. 2, 1–7. https://doi.org/10.5194/esurf-2-1-2014. https://doi.org/10.5194/esurf-2-1-2014

Shahid, M., Rahman, K.U., Haider, S., Gabriel, H.F., Khan, A.J., Pham, Q.B., Mohammadi, B., Linh, N.T.T. and Anh, D.T., 2021. Assessing the potential and hydrological usefulness of the CHIRPS precipitation dataset over a complex topography in Pakistan. Hydrological Sciences Journal, 66(11), pp.1664-1684. https://doi.org/10.1080/02626667.2021.1957476

Shahzad, F., Mahmood, S.A., Gloaguen, R., 2009. Drainage network and lineament analysis: An approach for Potwar Plateau (Northern Pakistan). J. Mt. Sci. 6, 14–24. https://doi.org/10.1007/s11629-009-0206-4 . https://doi.org/10.1007/s11629-009-0206-4

Formatted: Underline, Font color: Custom Color(RGB(17,85,204))

Formatted: Underline, Font color: Custom Color(RGB(17,85,204))

Formatted: Underline, Font color: Custom Color(RGB(17,85,204))

Formatted: Underline, Font color: Custom Color(RGB(17,85,204))

Formatted: Underline, Font color: Custom Color(RGB(17,85,204))

Formatted: Indent: Left: 0 cm, First line: 0 cm, Widow/Orphan control, Adjust space between Latin and Asian text, Adjust space between Asian text and numbers

Formatted: Indent: Left: 1.27 cm, Widow/Orphan control, Adjust space between Latin and Asian text, Adjust space between Asian text and numbers

Formatted: Underline, Font color: Custom Color(RGB(17,85,204))

Sharif, M., Archer, D.R., Fowler, H.J., Forsythe, N., 2013. Trends in timing and magnitude of flow in the Upper Indus Basin. Hydrol. Earth Syst. Sci. 17, 1503–1516. https://doi.org/10.5194/hess-17-1503-2013. https://doi.org/10.5194/hess-17-1503-2013

Sharma, S., Sati, S.P., Basavaiah, N., Pandey, S., Sundriyal, Y.P., Rana, N., Singh, P., Pradhan, S., Shukla, A.D., Bhushan, R., Bhatt, R., Juyal, N., 2022. Mid to late Holocene climate variability, forest fires and floods entwined with human occupation in the upper Ganga catchment, India. Quaternary Science Reviews 293, 107725. https://doi.org/10.1016/j.quascirev.2022.107725. https://doi.org/10.1016/j.quascirev.2022.107725

Sharma, S., Shukla, A.D., Bartarya, S.K., Marh, B.S., Juyal, N., 2017. The Holocene floods and their affinity to climatic variability in the western Himalaya, India. Geomorphology 290, 317–334. https://doi.org/10.1016/j.geomorph.2017.04.030. https://doi.org/10.1016/j.geomorph.2017.04.030

Sinha, R., Mohanta, H., Jain, V., Tandon, S.K., 2017. Geomorphic diversity as a river management tool and its application to the Ganga River, India. River Research & Apps 33, 1156–1176. https://doi.org/10.1002/rra.3154. https://doi.org/10.1002/rra.3154

Snyder, N.P., Whipple, K.X., Tucker, G.E., Merritts, D.J., 2003. Importance of a stochastic distribution of floods and erosion thresholds in the bedrock river incision problem. J. Geophys. Res. 108, 2001JB001655. https://doi.org/10.1029/2001JB001655. https://doi.org/10.1029/2001JB001655

Srivastava, P., Kumar, A., Chaudhary, S., Meena, N., Sundriyal, Y.P., Rawat, S., Rana, N., Perumal, R.J., Bisht, P., Sharma, D., Agnihotri, R., Bagri, D.S., Juyal, N., Wasson, R.J., Ziegler, A.D., 2017. Paleofloods records in Himalaya. Geomorphology 284, 17–30. https://doi.org/10.1016/j.geomorph.2016.12.011. https://doi.org/10.1016/j.geomorph.2016.12.011

Starke, J., Ehlers, T.A., Schaller, M., 2020. Latitudinal effect of vegetation on erosion rates identified along western South America. Science 367, 1358–1361. https://doi.org/10.1126/science.aaz0840. https://doi.org/10.1126/science.aaz0840

Formatted: Underline, Font color: Custom Color(RGB(17,85,204))

Formatted: Underline, Font color: Custom Color(RGB(17,85,204))

Formatted: Underline, Font color: Custom Color(RGB(17,85,204))

Formatted: Underline, Font color: Custom Color(RGB(17,85,204))

Formatted: Underline, Font color: Custom Color(RGB(17,85,204))

Formatted: Underline, Font color: Custom Color(RGB(17,85,204))

Formatted: Underline, Font color: Custom Color(RGB(17,85,204))

Tibau, X.-A., Reimers, C., Gerhardus, A., Denzler, J., Eyring, V., Runge, J., 2022. A spatiotemporal stochastic climate model for benchmarking causal discovery methods for teleconnections. Environ. Data Science 1, e12. https://doi.org/10.1017/eds.2022.11. https://doi.org/10.1017/eds.2022.11

Ullah, W., Wang, G., Lou, D., Ullah, S., Bhatti, A.S., Ullah, S., Karim, A., Hagan, D.F.T. and Ali, G., 2021. Large-scale atmospheric circulation patterns associated with extreme monsoon precipitation in Pakistan during 1981–2018. *Atmospheric Research*, *253*, p.105489. https://doi.org/10.1016/j.atmosres.2021.105489

Vellore, R.K., Kaplan, M.L., Krishnan, R., Lewis, J.M., Sabade, S., Deshpande, N., Singh, B.B., Madhura, R.K., Rama Rao, M.V.S., 2016. Monsoon-extratropical circulation interactions in Himalayan extreme rainfall. Clim Dyn 46, 3517–3546. https://doi.org/10.1007/s00382-015-2784-x. https://doi.org/10.1007/s00382-015-2784-x

Wang, N., Zeng, X.-M., Guo, W.-D., Chen, C., You, W., Zheng, Y., Zhu, J., 2018. Quantitative diagnosis of moisture sources and transport pathways for summer precipitation over the mid-lower Yangtze River Basin. Journal of Hydrology 559, 252–265. https://doi.org/10.1016/j.jhydrol.2018.02.003. https://doi.org/10.1016/j.jhydrol.2018.02.003

Whipple, K.X., Hancock, G.S., Anderson, R.S., 2000. River incision into bedrock: Mechanics and relative efficacy of plucking, abrasion, and cavitation. Geological Society of America Bulletin 112, 490–503. https://doi.org/10.1130/0016-7606(2000)112<490:RIIBMA>2.0.CO;2. https://doi.org/10.1130/0016-7606(2000)112<490:RIIBMA>2.0.CO;2

Whipple, K.X., Tucker, G.E., 1999. Dynamics of the stream-power river incision model: Implications for height limits of mountain ranges, landscape response timescales, and research needs. J. Geophys. Res. 104, 17661–17674. https://doi.org/10.1029/1999JB900120. https://doi.org/10.1029/1999JB900120

Wobus, C., Whipple, K.X., Kirby, E., Snyder, N., Johnson, J., Spyropolou, K., Crosby, B., Sheehan, D., 2006. Tectonics from topography: Procedures, promise, and pitfalls, in: Tectonics, Climate, and Landscape Evolution. Geological Society of

Formatted: Indent: Left: 0 cm, First line: 0 cm, Widow/Orphan control, Adjust space between Latin and Asian text, Adjust space between Asian text and numbers

Formatted: Indent: Left: 1.27 cm, Widow/Orphan control, Adjust space between Latin and Asian text, Adjust space between Asian text and numbers

Formatted: Underline, Font color: Custom Color(RGB(17,85,204))

Formatted: Underline, Font color: Custom Color(RGB(17,85,204))

Formatted: Underline, Font color: Custom Color(RGB(17,85,204))

Formatted: Underline, Font color: Custom Color(RGB(17,85,204))

America. https://doi.org/10.1130/2006.2398(04) . https://doi.org/10.1130/2006.2398(04)

Wolfensberger, D., Gabella, M., Boscacci, M., Germann, U., Berne, A., 2021. RainForest: a random forest algorithm for quantitative precipitation estimation over Switzerland. Atmos. Meas. Tech. 14, 3169–3193. https://doi.org/10.5194/amt-14-3169-2021 . https://doi.org/10.5194/amt-14-3169-2021

Wu, K., Liu, S., Jiang, Z., Liu, Q., Zhu, Y., Yi, Y., Xie, F., Ahmad Tahir, A., Saifullah, M., 2021. Quantification of glacier mass budgets in the Karakoram region of Upper Indus Basin during the early twenty-first century. Journal of Hydrology 603, 127095. https://doi.org/10.1016/j.jhydrol.2021.127095 . https://doi.org/10.1016/j.jhydrol.2021.127095

Zeitler, P.K., Koons, P.O., Bishop, M.P., Chamberlain, C.P., Craw, D., Edwards, M.A., Hamidullah, S., Jan, M.Q., Khan, M.A., Khattak, M.U.K., Kidd, W.S.F., Mackie, R.L., Meltzer, A.S., Park, S.K., Pecher, A., Poage, M.A., Sarker, G., Schneider, D.A., Seeber, L., Shroder, J.F., 2001. Crustal reworking at Nanga Parbat, Pakistan: Metamorphic consequences of thermal-mechanical coupling facilitated by erosion. Tectonics 20, 712–728. https://doi.org/10.1029/2000TC001243 . https://doi.org/10.1029/2000TC001243

Zeitler, P.K., Meltzer, A.S., Brown, L., Kidd, W.S., Lim, C., Enkelmann, E., 2014. Tectonics and topographic evolution of Namche Barwa and the easternmost Lhasa block, Tibet, in: Toward an Improved Understanding of Uplift Mechanisms and the Elevation History of the Tibetan Plateau. Geological Society of America Special Papers, pp. 23–58.

Formatted: Underline, Font color: Custom Color(RGB(17,85,204))

Formatted: Underline, Font color: Custom Color(RGB(17,85,204))

Formatted: Underline, Font color: Custom Color(RGB(17,85,204))

Formatted: Underline, Font color: Custom Color(RGB(17,85,204))

Formatted: Font: 11 pt

Formatted: Justified, Indent: Left: 0 cm, First line: 0 cm, Space Before: 12 pt, After: 12 pt, Widow/Orphan control, Adjust space between Latin and Asian text, Adjust space between Asian text and numbers